Near Wellbore Salt Precipitation in Gas Reservoirs

Rohith Nair

Master of Science Thesis

TU Delft Delft University of Technology

TNO innovation for life

Near Wellbore Salt Precipitation in Gas Reservoirs

Master of Science Thesis

For the degree of Master of Science in Applied Earth Sciences at Delft University of Technology

Rohith Nair

September 24, 2015

Section for Petroleum Engineering · Delft University of Technology

Delft University of Technology
Department of
Geoscience & Engineering

The undersigned hereby certify that they have read and recommend to the Section for Petroleum Engineering for acceptance a thesis entitled

Near Wellbore Salt Precipitation in Gas Reservoirs

by

Rohith Nair

in partial fulfillment of the requirements for the degree of

Master of Science Applied Earth Sciences

Dated: September 24, 2015

Supervisor(s):

prof.dr.ir. P.L.J. Zitha

Dr.ir. P.J.P. Egberts

Reader(s):

Dr.ir. K.H.A.A. Wolf

prof.dr.ir. J.Bruining

Dr.ir. A. Twerda

Abstract

Production wells in gas reservoirs often experience rapid production decline towards the late production stage. In many cases, this behavior can be attributed to salt precipitation in the near wellbore region. Water evaporates in the vicinity of the well bore with pressure drop, leading to an increase in the dissolved salt concentration, causing salt precipitation when the solubility limit is exceeded. Salt deposition causes the blockage of gas flow in the vicinity of the wellbore and increases towards the end of lifetime of a gas field, thus becoming problematic for most North Sea assets.

Regular downhole fresh water treatments are required to restore the production back to normal. However, these water treatments are expensive and are required quite frequently. Thus, a better understanding of this phenomenon and the conditions under which it takes place is necessary. Additionally, the question arises whether there exists a better reservoir management strategy that can can improve control over well productivity.

The model used to model salt precipitation in this work is a compositional two-phase N-component porous media flow model under isothermal conditions(2pNcmin) developed in the numerical simulator DuMu^X.

A sensitivity analysis was carried out to measure the sensitivity of the model to certain critical parameters and to understand the phenomenon better. The concept of a drying-transport balance was then developed, which can help understand the salt precipitation trends occurring under differing conditions.

A study of the variables controlling the productivity of wells plagued by salt precipitation shows that there does exist an optimized reservoir management strategy which can better the cash flow from such wells. Based on these results, a simplified analytical model was developed to show the scope for optimization. Furthermore, an optimization problem was formulated to maximize the Net Present Value (NPV) of wells undergoing cyclic production and water washing.

Table of Contents

List of Figures

List of Tables

Acknowledgements

First and foremost I am truly grateful to my supervisor, Dr. Paul Egberts, who has supported me throughout my thesis with his patience and knowledge, whilst allowing me the room to work and develop in my own way. He has taught me both consciously and unconsciously how good research is done. I attribute most of my learning during this work, to the insightful discussions we had on a variety of topics.

I sincerely thank Prof. P.L.J. Zitha for supervising my work, for his valuable insights and constructive feedback and for providing me the opportunity to work with TNO on such an interesting topic. The support and cooperation offered by TNO in realizing this thesis is gratefully acknowledged. I would also like to thank the entire HTFD department of TNO for making my 8 months here very comfortable. Furthermore, I am very grateful to the "salt precipitation" group within TNO, for helping me with my work and for taking time off their busy schedules to answer my many questions.

I am thankful to Dr. Vishal Jambhekar and Dr. Bernd Flemisch for their timely help with the numerical simulator DuMu^X. Without their help and counsel, this work would have been immeasurably more difficult.

I would like to warmly thank Dr. Ivan Garcia for teaching me essentially everything I know about Linux and for providing an experienced ear for most of my programming related doubts. I am also indebted to the University of Stuttgart and to the 'Open Source' programming community for providing the tools I have used to produce both my results and this thesis.

I have been blessed with a helpful and cheerful group of friends, both at work and home, who have motivated me throughout the duration of my thesis and have helped me right from designing graphics, to working with LaTeX and to data management. My special thanks go out to all of them for making my stay in Delft memorable.

Finally, I would like to express my love and gratitude to my family. I owe all my success in life to my parents for always believing in me, for being a constant in an ever-changing world and for being ever supportive of my thirst for learning.

Delft, University of Technology — Rohith Nair
September 24, 2015

Chapter 1

Introduction

This thesis addresses the phenomenon of salt precipitation in gas reservoirs and the scope of optimizing the gas production from such reservoirs to maximize productivity. This chapter gives an overview of the salt precipitation problem and the motivation behind the research question of this thesis.

Salt precipitation in geological formations is a growing concern and a problem plaguing many mature gas producing wells in the North Sea. This phenomenon can negatively affect the performance of production and injection wells. Gas production wells have been found to experience rapid decline in productivity towards their late life, due to salt precipitation near the well bore. In many cases this can even result in well shut down due to plugging of the perforations and near wellbore clogging Place and Smith [1984]. Periodic downhole fresh water treatments are currently being used to dissolve precipitated salt and restore productivity of the well. However, these water treatments are expensive and are required quite frequently. This poses the question whether there exists a better reservoir management strategy that can minimize the productivity loss due to salt precipitation. Salt precipitation thus poses a major problem for exploiting the maximum potential of a gas reservoir. The mechanisms underlying the phenomenon and the possibility of an optimized reservoir management strategy thus needs to be investigated further.

Gas reservoirs contain a large volume of water in the form of formation water (Fig. 1-1a). Formation water salinity generally increases with depth of the reservoir and can contain large volumes of dissolved salts. During gas production, this water is removed from the reservoir due to a combination of immiscible displacement, advection and evaporation. These water removal mechanisms work in parallel and their effect on the porous medium is collectively known as drying. Furthermore, the effect of evaporation in the drying process becomes increasingly important as the aqueous phase becomes immobile. A reduction in water saturation due to evaporation results in an increase of the salt ion concentration. “Salt deposition occurs when the solubility product of the dissolved ions is exceeded either because of evaporation or dissolution of rock” Le and Mahadevan [2011]. As drying progresses, the salinity of the reservoir increases, and halite precipitation ensues when the salinity of the formation water reaches the solubility limit (Fig. 1-1b). Formation waters containing a high value of Total

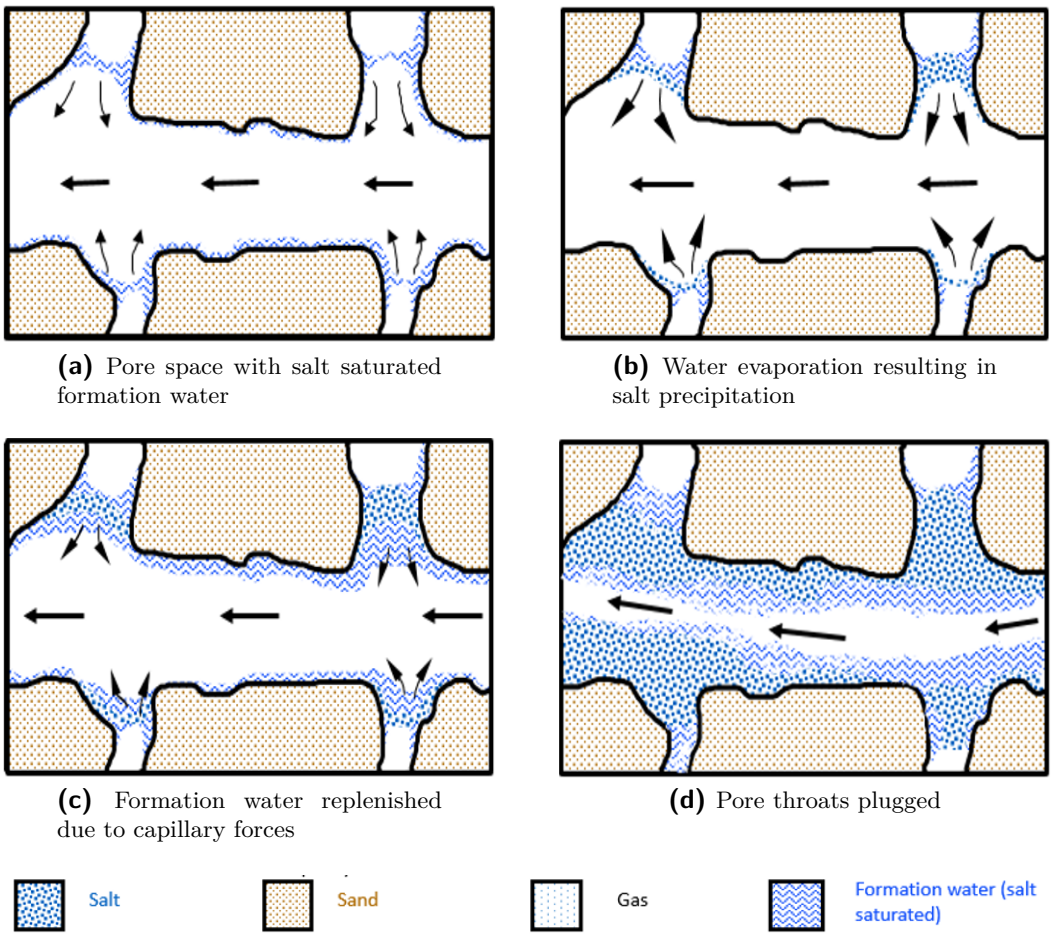

(a) Pore space with salt saturated formation water

(b) Water evaporation resulting in salt precipitation

(c) Formation water replenished due to capillary forces

(d) Pore throats plugged

Figure 1-1: Pore scale schematic of the salt precipitation process (from Mobil [2011])

Dissolved Solids (TDS) content can potentially result in substantial volumes of precipitated salts. Additionally, the amount of salt precipitated has been found to depend heavily on the formation water salinity and water transport, as shown in Fig. 1-1c. There is a reduction in rock porosity associated with the deposition of salt. The resulting reduction in absolute permeability depends on the porosity-permeability relationship characteristic to the formation. The formation of this altered permeability zone near the well causes an additional pressure drop, which leads to a decline in gas production and can lead to complete clogging of the pore throats (Fig. 1-1d), when the permeability drops to zero.

A review of literature shows that there are a few techniques that can mitigate the effect of salt precipitation, when used. These are:

- Downhole fresh water treatments
- Usage of salt inhibitors
- Hydraulic fracturing of the near wellbore area

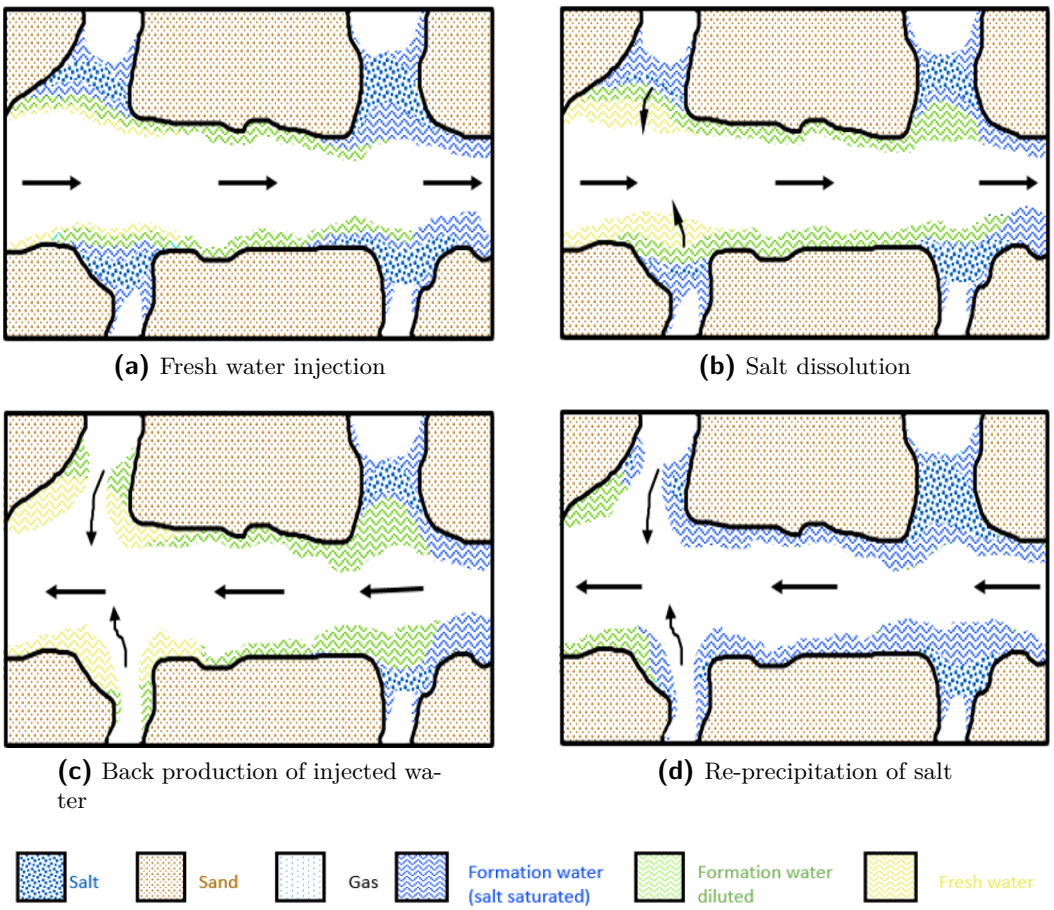

Figure 1-2: Pore scale schematic of the water washing process (from Mobil [2011])

Periodic downhole fresh water treatments (or water washes) are currently being used by the operators of the gas fields in the North Sea, to wash away precipitated salt in the near-wellbore region. These water washes dissolve the salt precipitated near the wellbore and return the reservoir to its unaltered permeability state (Fig. 1-2a, 1-2b). However, salt starts re-precipitating once the injected water has been produced back (Fig. 1-2c, 1-2d). According to field observations, the frequency with which water washes are required, to maintain well productivity, increases during the lifetime of the reservoir. Furthermore, water washes are expensive and can be logistically challenging in certain cases. This calls for a study to find out whether there exists a better reservoir management strategy, which can optimize the productivity of gas reservoirs with a salt precipitation issue.

This report addresses the phenomenon of salt precipitation in gas reservoirs, with a focus on the influence of liquid transport and drying rates on the precipitation profile. The objective of this thesis is to provide a hypothesis which can give the reason behind the differing locations of salt precipitation observed during various reservoir simulations. A parallel objective is to explore the possibility of optimizing the reservoir management strategy to minimize the productivity loss from salt precipitation.

The theory and concepts underlying the salt precipitation phenomenon are introduced in

chapter 2. Chapter 3 describes the concept of the model developed in the open source simulator 'DuMu^X' and its implementation. Chapter 4 introduces the Drying–Transport balance hypothesis, which has been developed to help understand the location and rate of salt precipitation. Since the salt precipitation phenomenon is very sensitive to some parameters, a sensitivity analysis has been carried out in this chapter. These sensitivities have also been interpreted using the drying-transport balance hypothesis. Chapter 5 builds on the results obtained the previous chapter to build a optimization model and goes on to formulize an optimization problem which can better the reservoir management and production strategy for reservoirs with the salt precipitation issue.

Chapter 2

Brine Flow and Salt Precipitation in Porous Media

2-1 Salt Precipitation Literature

Salt deposition in natural gas reservoirs occur when the solubility product of the dissolved Na^+ and Cl^- ions is exceeded either because of water evaporation or dissolution of the rock Le and Mahadevan [2011].

A review of literature shows us that there are a few mechanisms that can result in salt precipitation. One of the dominant mechanisms is the evaporation of formation water into the producing gas stream, which in turn increases the salt ion concentration and thus results in precipitation above the solubility limit. Moreover, the pressure and temperature of a petroleum reservoir changes during its producing life and this influences the amount of water vaporization and can also affect the solubility of salt in the formation water. Dullien et al. [1989], Holditch [1979], Kamath and Laroche [2003], showed that the evaporation regime during flow-through-drying sets in only after an initial viscous displacement. Dietzel et al. [1993], mentions that a decrease in reservoir pressure could result in an expansion of the formation water to saturations above irreducible and could explain continued salt transport and precipitation.

Recently, some work has been carried out to determine the location of salt precipitation. In their study, Kleinitz et al. [2001] concluded that apart from the reservoir, salt can accumulate in the well bore and perforation zone as well. Majority of the flow-through-drying experiments carried out, report observations of precipitation near the core outlet or in the context of a natural gas reservoir, near-wellbore precipitation. van Dorp et al. [2009], in their numerical and experimental investigation on flow-through-drying in a laboratory sand pack under radial flow conditions, report higher NaCl concentrations near the outlet of the sand pack. A review of literature shows that various analysis have been provided to reason for the location of salt precipitation. Le and Mahadevan [2011], concludes that during the flow of a saturated gas, evaporation occurs due to gas expansion caused by the pressure drop near the

wellbore region. Mahadevan et al. [2007], argues that capillary wicking (or capillary driven film flow) is a significant mechanism for the transport of salt to near wellbore regions, leading to near wellbore salt clogging. In their study, Newsham and Rushing [2009] states that water vaporization occurs during gas production due to the increase in water partial pressure, as the reservoir gas pressure declines in the vicinity of the well bore and that the water moisture content in the gas is a function of pressure, temperature, gas velocity and brine salinity. Tang and Etzion [2004] developed empirical relationships for evaporation of water from a wetted surface and suggests that higher gas velocities results in higher evaporation rates, while Zuluaga and Monslave [2003] indicates that water evaporation rate increases with gas flow rate and decreases with salinity. Additionally, van Dorp et al. [2009] suggests that in a homogeneous reservoir pore clogging occurs near the wellbore, since the pore volume is the minimum in this region.

The phenomenon of flow-through drying, evaporation in porous media and capillary film flow are explored further in the subsequent sections.

2-2 Flow-Through Drying

Drying is defined as a "mass transfer process consisting of the removal of water or another solvent by evaporation from a solid, semi-solid or liquid" Greensmith [1998]. Drying in subsurface porous media usually takes place due to the flow of a gas(saturated or dry) over or through a porous medium partially occupied by an aqueous phase.

Several studies have been conducted on the drying of porous media. The majority of these studies focus on the flow of an unsaturated gas over a wetted porous media, which leads to evaporation of the wetting liquid into the unsaturated gas Mahadevan et al. [2006]. These studies thus focus on diffusion driven drying, where the evaporation is driven purely by the gradient in moisture content of the gas.

A different way of studying drying in porous media is flow-through drying. Flow-through drying takes place when a gas(saturated or dry) phase is injected into or flows through a porous medium partially occupied by an aqueous phase. Removal of the liquid phase during flow-through drying occurs due to the combination of immiscible liquid displacement due to viscous pressure drop and evaporation of the aqueous phase. Allerton et al. [1949], concluded from their experiments with dry gas injection that the evaporation regime sets in only after an initial immiscible displacement regime. Evaporation is largely responsible for the drying up of porous media, after the liquid phase becomes immobile Mahadevan and Sharma [2005].

When the gas injected or passed through is fully saturated, evaporation cannot take place without gas expansion, since there is no gradient in moisture content. In this case, flow-through drying has been found to be heavily influenced by gas compressibility and capillarity. Compressibility driven evaporation occurs when there exists a pressure drop resulting in gas expansion, which leads to diffusion driven evaporation. Capillarity facilitates the redistribution of liquid from regions of low drying rates to regions with higher drying rates, through macroscopic capillary film flows, thus accelerating the drying process Mahadevan et al. [2006]. Higher pressure drops, hydrophobicity of the pore surface and solvent addition were shown to improve evaporation efficiency Mahadevan and Sharma [2005]. Multiple models have been developed to describe the drying process in porous media.

Luikov [1966], Whitaker and Chou [1983], developed a drying theory based on volume averaging methods. Efforts were also made to conduct pore network studies, to describe drying as a drainage process controlled by the diffusion of evaporating gas to the external surface, while including the effect of liquid counter flow through macroscopic films along pore walls. Yiotis et al. [2004], presented a pore-network model that included corner films to account for such counter-flows and showed that depending on the capillary properties of the rock, the presence of macroscopic films can significantly affect the drying rates.

Gas in natural gas reservoirs with associated water is initially saturated with water vapor. The process of gas production can thus be seen as the flow of saturated gas through a porous medium partially occupied by an aqueous phase. Large pressure gradients near the producer well leads to gas expansion and cause evaporation of water. The phenomenon of salt precipitation in gas reservoirs can thus be interpreted as a result of flow-through drying. A continuum model with volume averaged properties is used to model the drying process in DuMu^x. The process of evaporation is explained in section 2-3.

2-3 Evaporation in Porous Media

Evaporation is vaporization of a liquid phase into the gas phase. The conditions required of molecules in a liquid to evaporate are that they must be located near the liquid-gas interface, be moving in the proper direction, and have sufficient kinetic energy to overcome liquid-phase intermolecular forces. The number of molecules which fulfil these conditions determines the rate of evaporation. The rate of evaporation is low when only a small proportion of molecules satisfy these conditions. Furthermore, evaporation proceeds quicker at higher temperatures, since the kinetic energy of a molecule is proportional to its temperature.

2-3-1 Stages of Evaporation

Pure Water Evaporation

Based on the previous studies by Coussot [2000], Fisher [1923], Nachshon et al. [2011] and Lehmann et al. [2008], the evaporation of pure water from a homogeneous porous media has been demarcated into the following three stages:

- Stage 1 (S1): A relatively constant and high evaporation rate is characteristic of this stage. The evaporation during this stage is capillary-driven and continues as long as there exists hydraulic connectivity between the receding drying front and the free-flow-porous-media interface, which is necessary to sustain a high evaporation rate.
- Stage 2 (S2): This stage begins when the evaporation front lowers further and the hydraulic conductivity between the pores is disturbed. During this stage, evaporation is restricted by vapor diffusion in the porous medium.
- Stage 3 (S3): This stage is established when the evaporation front is far below the free-flow-porous-media interface. A low evaporation rate governed only by diffusive vapor transport is characteristic of this stage.

Brine Water Evaporation

Gas reservoirs contain water in the form of formation water. Formation water can contain considerable amounts of dissolved salts. It is therefore important to understand the impact of dissolved salt distribution, accumulation and precipitation on evaporation dynamics. Shimojimaa et al. [1996], Nassar and Horton [1999], Fujimaki et al. [2006], studied the effect of salt crust formation and salt precipitation on the evaporation dynamics in porous media, albeit in the context of soil salinization. Additionally, Nachshon et al. [2011] studied saline water evaporation dynamics in heterogeneous media and defined three new stages of evaporation for saline solutions. These are:

- Stage 1 (SS1): An initially high evaporation rate with small reductions due to increase in osmotic potential, is characteristic of this stage. Osmotic potential increases as a consequence of the increasing salt concentration in the solution, due to evaporation.
- Stage 2 (SS2): As a result of pore clogging due to salt precipitation and loss of hydraulic connectivity, to the porous media surface, evaporation rate falls sharply during this stage.
- Stage 3 (SS3): This stage displays a constant low rate of evaporation rate governed by diffusion of water vapor across the precipitated salt crust in the porous media.

Numerical modelling of saline water evaporation is difficult when compared to pure water evaporation. This is because the dissolved salt transport distribution, the fluctuation in vapor pressure and salt precipitation and its effect of evaporation dynamics have to be modelled in addition to the evaporation process. Furthermore, changes in the pore geometry related to salt precipitation affect porous media properties. The comparison of evaporation rate between pure water evaporation and brine water evaporation is given in Fig. 2-1.

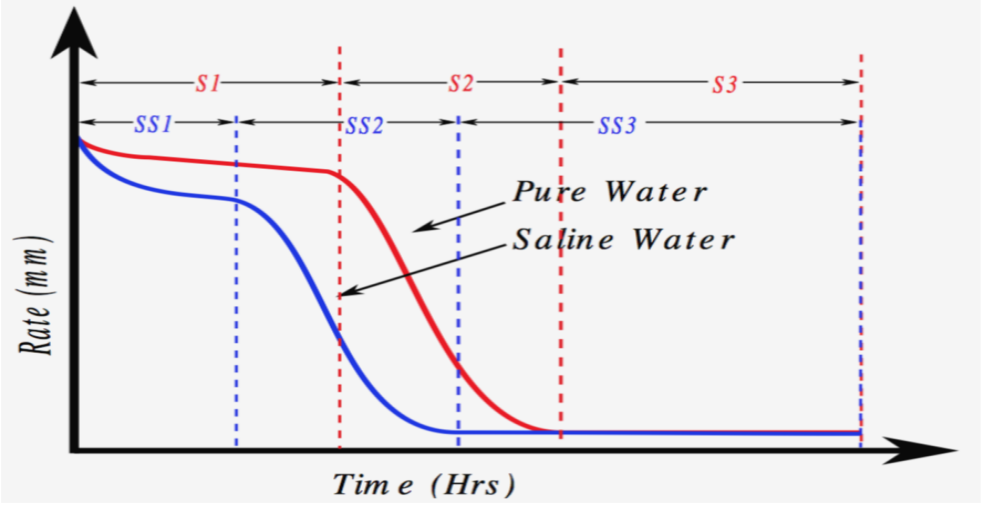

Figure 2-1: Schematic representation of the stages and inter stage transition for pure-water and saline-water evaporation (from Jambhekar et al. [2015])

2-3-2 Vapor Pressure Lowering

Vapor pressure lowering is a colligative property of solutions. The vapor pressure of a pure solvent is greater than the vapor pressure of a solution containing a non volatile liquid. This lowered vapor pressure leads to boiling point elevation. Furthermore, in porous media, vapor pressure lowering also takes place due to the effects of capillarity and vapor adsorption.

Salinity Dependent Vapor Pressure Lowering

A liquid containing more than one component has a lowered vapor pressure for each of its components. This lowering in vapor pressure, due to the addition of a non-volatile solute to a solution is described by the Raoult's law to be proportional to the mole fraction of the component in the liquid phase.

$$P_g^{H_2O} = X_l^{H_2O} P_{g,sat}^{H_2O} \tag{2-1}$$

Here, $P_{g,sat}^{H_2O}$ is the vapor pressure of the pure liquid, $P_g^{H_2O}$, the vapor pressure and $X_l^{H_2O}$ is the mole fraction of water in the liquid phase. Mixtures in which Raoult's law is valid for all mole fractions are called ideal.

Suction Pressure Dependent Vapor Pressure Lowering

Vapor pressure lowering in porous media can take place due to the effect of capillary pressure and surface adsorption. Here, capillary pressure and vapor adsorption effects are referred to as suction pressure effects. Vapor pressure lowering due to suction pressure, originates due to the deviation of the liquid interface from a flat surface. The curvature of the liquid surface will be concave at low liquid saturations. The partial pressure of vapor above a concave interface is lower than above a flat surface, and thus the lowering in vapor pressure.Vapor pressure lowering due to suction pressure is described by Battistelli et al., by the relation:

$$P_g^{H_2O} = f_{VPL} P_{g,sat}^{H_2O}, \tag{2-2}$$

The vapor pressure lowering factor(f_{VPL}) is given by the Kelvin's equation as:

$$f_{VPL} = exp\left[\frac{W^{H_2O} p_c}{\rho_l R T}\right], \tag{2-3}$$

where W^{H_2O} is the molecular weight of water (kg/mol), p_c is the capillary pressure, R, the gas constant and T, the temperature.

From their simulations on drying of porous media, Battistelli et al. observed that inclusion of vapor pressure lowering due to suction pressure prevents complete dry-out of the porous medium. Furthermore, Pruess and Sullivan from their study of VPL effects in vapor-dominated reservoirs, states that the suction pressure required for a vapor pressure lowering of 1%, 10% and 20% are 19.4 bar, 203 bar and 430 bar, respectively. Thus, a significant reduction in vapor pressure is observed only for very high suction pressure values.
The salt precipitation model used in this work neglects the effect of suction pressure on vapor pressure lowering.

2-4 Capillary Film Flow

The water saturation in the non-hygroscopic region of a porous media varies from 1 to 0 Goyeneche et al. [2002]. The term non-hygroscopic refers to regions in the porous media, where water is unable to be adsorbed or desorbed on to the solid skeleton. A review of the literature suggests that this region is often sub-divided into two zones called '*funicular*' and '*pendular*', separated by the point of irreducible saturation at which $S = S_{irr}$ Spolek and Plumb [1981], Whitaker and Chou [1983], Kaviany and Mittal [1987] and Perre and Moyne [1991], Puiggali and Quintard [1992]. The former refers to the regions where the water saturation is above irreducible saturation and the latter, below. The existence of such a point, above which free water remains continuous and below which it would be discontinuous, could be justified by the work performed by Comstock [1970], Spolek and Plumb [1981]. It was assumed that liquid flow could not occur in the pendular zone and that liquid flow would occur in the funicular region, due to presence of hydraulic connectivity. However, Whitaker and Chou [1983], raised strong arguments to show that the mechanisms of diffusive vapor transfer in the gas phase and convective transport of humid air were alone not sufficient to explain the rate of water removal in the pendular zone. Additionally, further research by Moyne [1987], confirmed the previous speculations that there is a liquid phase mass transfer occurring below the irreducible saturation. This was thought possible if the liquid phase remains connected in the pendular zone, through connected wetting liquid films. Yiotis et al. [2004], from their investigation on the effect of liquid films on the drying of porous media, have concluded that film flow in porous media exists and is a major transport mechanism, which becomes dominant when capillarity controls the drying process.

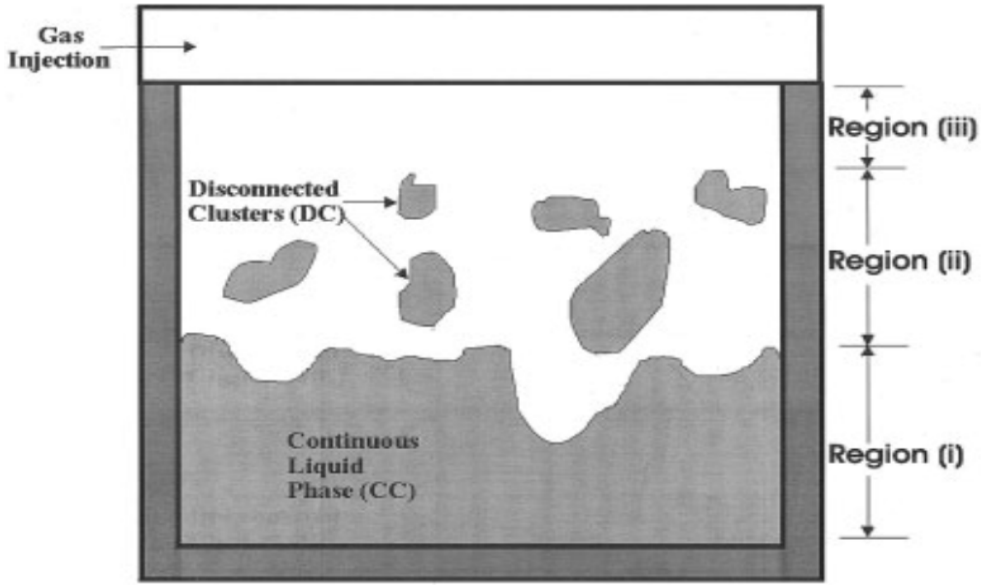

Figure 2-2: Drying of a liquid in a porous medium (from Yiotis et al. [2004])

Drying is a drainage process, wherein the evaporating wetting liquid is being displaced by a non-wetting gas. The typical geometry of an isothermal drying application is shown in Fig. 2-2. Evaporative drying results in the reduction of liquid saturation below irreducible. Due to this inconsistency in the definition of the irreducible saturation, Mahadevan et al. [2006]

termed this saturation as the "apparent residual saturation". Additionally, the phenomenon of capillary driven film flow was termed as "wicking". Furthermore, due to the reduction in water saturation below the apparent irreducible, one unique aspect of drying is the presence of disconnected clusters (DC) of the liquid [region (ii) in Fig. 2-2], which develops in front of the main continuum liquid cluster (CC) [region (i) in Fig. 2-2]. The patterns of the continuous and discontinuous phases and the rate of displacement of liquid is controlled by the mass transfer in the gas phase Yiotis et al. [2004]. According to Yiotis et al. [2004], the pore space can be characterized into three kinds, in the presence of wetting films, at any stage of the drying process. These kinds of pores are as shown in Fig. 2-3: type-L pores, fully occupied by liquid; type-G pores, fully occupied by gas; and type-F pores, occupied by gas, but also containing liquid films. Furthermore, in the work of Yiotis et al. [2004], attention has been restricted to "thick" films. This was because thin films, with thicknesses of the order of nanometers were found to have very low hydraulic conductivity, and thus their contribution to the overall liquid flow in drying would be negligible compared to that of thick films.

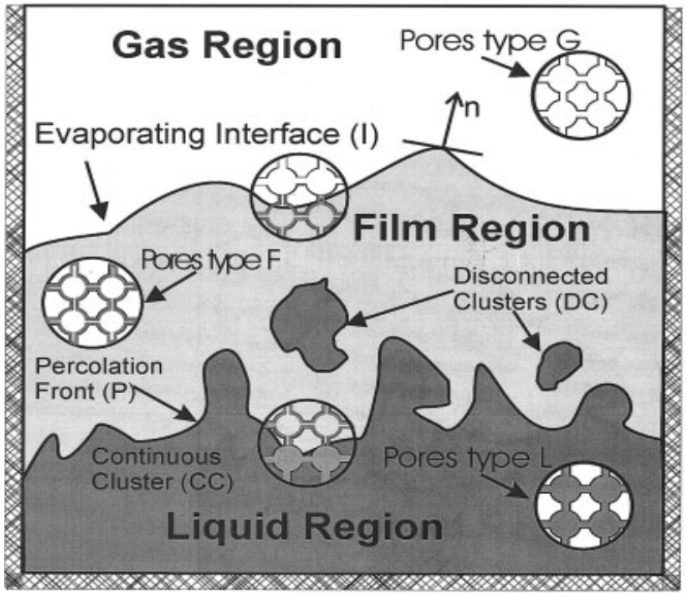

Figure 2-3: Types of pore spaces present during drying (from Yiotis et al. [2004])

It is quite important to understand how to model the capillary pressure and relative permeability curves below this 'apparent residual saturation', for the purposes of salt precipitation in gas reservoirs. However it is unclear from literature on how these curves have to be regularized.

According to Ward and Morrow [1987], capillary pressures below the irreducible saturation can be calculated using the kelvin equation, which relates the difference in vapor pressure, to the curvature across the interface of a liquid ring or bridge in porous media. Since the gas phase typically contains more than one component and is not exclusively water vapor, this assumption does not hold true for all cases. Relative permeability for gas is generally easily measured below the irreducible saturation and correlations are available from experimental data reported in literature. However, water relative permeabilities below the irreducible saturation are not easily obtained, because liquid mobilities are extremely low and are often

orders of magnitudes lower than gas relative permeabilities Ward and Morrow [1987]. Water phase relative permeability is thus usually represented by empirical relationships.

Le and Mahadevan [2011] assumes that below the apparent residual saturation, the driving force for transport through these films is the pressure gradients caused by the interfacial curvature gradients. Furthermore, they developed a relative permeability relationship below the threshold saturation using the concept of liquid film flow, based on the assumption by Yiotis et al. [2004], that thick wetting films control the distribution and transport of liquid within the pore spaces of the rock. The modifications carried out to the capillary pressure, water and gas relative permeability curves by Le and Mahadevan [2011], to account for film flow below the apparent residual saturation is as given below.

2-4-1 Capillary Pressure Correction

The modified Van Genuchten model has been used to describe the capillary pressures. The normalized water saturation used in the expression was replaced by the water saturation to capture the capillary pressure for saturations below the apparent residual. The equation for capillary pressure is as follows:

$$p_c = \frac{1}{\alpha^{'}}[(S_w)^{-\frac{1}{m}} - 1]^{\frac{1}{n}}, \tag{2-4}$$

where parameters $m = 1 - \frac{1}{n}$ and $\alpha^{'}$ are obtained through curve fitting actual capillary pressure measurements and S_w is the water saturation.

2-4-2 Gas Relative Permeability Correction

A power law has been used to represent the relative permeability of gas:

$$k_{rg} = k^0_{rg}(1 - S_w)^{n_g}, \tag{2-5}$$

where, n_g is a positive exponent and k_{rg} is the relative permeability of gas.

2-4-3 Water Relative Permeability Correction

The water relative permeability for saturations above the apparent residual was modelled using a Corey-type relationship:

$$k_{rw} = k^0_{rw}\bar{S_w}^{n_w}, \tag{2-6}$$

where n_w is a positive exponent, $\bar{S_w}^{n_w}$ is the effective saturation defined in equation 3-15 and k_{rw} is the relative permeability of water.

The models developed by Laroche et al. [2004], uses thick corner flow physics for near-residual saturations and thin film physics for extremely low saturations. For liquid saturations below the apparent residual, the corner flow model by Mahadevan et al. [2006], gives a square relationship between the water relative permeability and the water saturation:

$$k_{rw} = BS_w^2, \tag{2-7}$$

where B is a constant that is yet to be determined. Fig. 2-4 depicts the regularization of relative permeabilities below the apparent residual saturation, carried out by
Le and Mahadevan [2011]. The apparent residual saturation and end point water relative permeability calculated in this example is approximately 0.5 and 0.23 respectively.

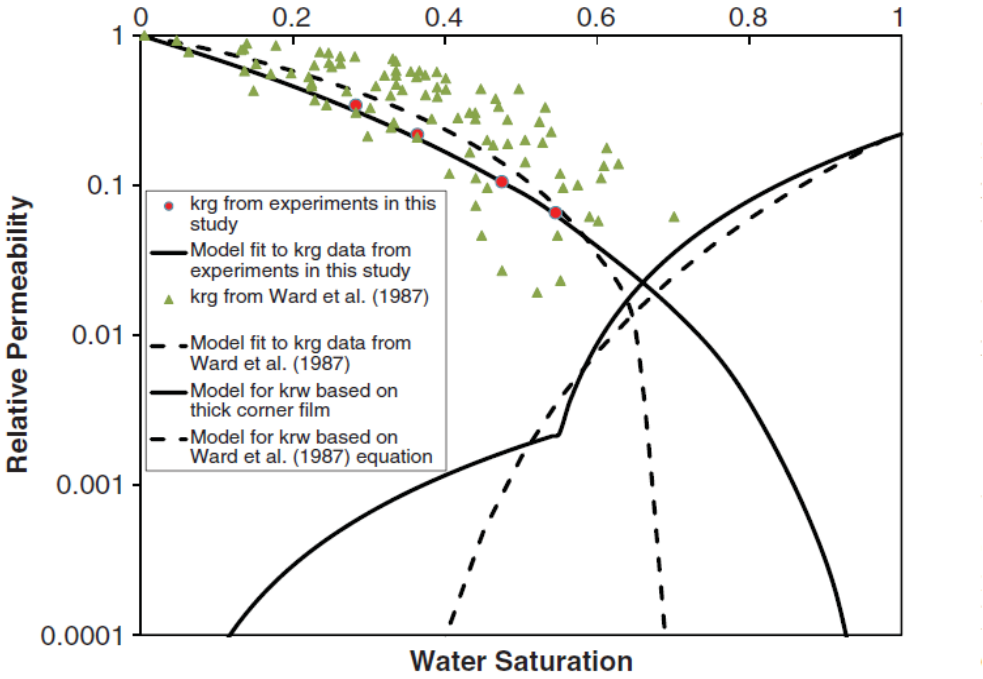

Figure 2-4: Plot of relative permeability measurements by Ward and Morrow [1987] (green triangles), and data from Le and Mahadevan [2011] (red circles). The solid lines represent model fits to the data. Below the apparent residual saturation, the solid lines represents the liquid relative permeability calculated using the corner film model. The dashed lines represent relative permeabilities calculated from the emperical model presented by Ward and Morrow [1987] (from Le and Mahadevan [2011])

In order to model capillary film flow below the apparent residual saturation, the salt precipitation model used in this work utilizes a quadratic water relative permeability regularization similar to Eqn. 2-7.

Chapter 3

Modelling Salt Precipitation in DuMu^X

The modeling toolbox DuMu^X was chosen as the framework for the implementation of the numerical scheme required to model the salt precipitation process. DuMu^X is an open-source simulator based on continuum mechanical concepts, to simulate flow and transport processes in porous media. Furthermore, it is based on the Distributed and Unified Numerical Environment (DUNE), which is a modular toolbox for solving partial differential equations with grid-based methods Bastian et al. [2008]. The main intention of DuMu^X is to provide a sustainable and consistent framework for the implementation and application of model concepts, constitutive relations and discretization, Flemisch et al. [2011] with a focus on porous-medium applications.

The model being used to model salt precipitation is a compositional two-phase N-component porous media flow model under isothermal conditions(2pNcmin in DuMu^X). The N-component model is used so that the same model could subsequently be used to model precipitation of a combination of different dissolved salts. The two fluid phases are:

- **Liquid Phase:** This phase is composed of water (w) as its main component, gas (CH_4) and dissolved NaCl(s).
- **Gas Phase:** This phase is composed of two components, namely gas (CH_4) and water vapor (w).

3-1 Mathematical Model

In order to create a simplified mathematical model for the porous media, several assumptions are made. They are:

3-1-1 Assumptions

- The solid matrix is rigid (no change in porosity due to compaction) and inert.
- Both the liquid and gas phases are assumed to be Newtonian fluids
- Multiphase Darcy's law is valid since the flow is assumed to be slow and non-darcy effects are neglected
- Only binary diffusion is considered and dispersion caused by different flow velocities is ignored
- Local chemical equilibrium
- The effect of gravity has been neglected in all the simulations unless specified otherwise
- The reservoir is assumed to be homogenous and anisotropic
- The system is assumed to be isothermal
- Gas is assumed to be ideal
- Precipitated salt is considered to be immobile
- The capillary end effect is neglected
- The porous medium is assumed to be water wet
- Halite ($NaCl$) is the only salt dissolved in the formation water
- The fugacity of a component in each phase is the same
- The effect of dissolved CH_4 component is neglected in calculating the density of the liquid

3-1-2 Compositional Multiphase Flow

The porous media being considered consists of two fluid phases $\alpha \in \{l,\ g\}$. The liquid phase consists of a water (H_2O) component, gas (CH_4) and dissolved salt ($NaCl$), while the gas phase consists of a gas(CH_4) component and water vapor(H_2O). With the mole fraction x^k_α of component $k \in \{H_2O, CH_4, NaCl\}$ in a phase α and the phase saturation S_α, the mass conservation for each component is given $\forall k \in \{H_2O, CH_4, NaCl\}$ as:

$$\sum_{\alpha\in\{l,g\}} \frac{\partial(\phi\rho_{mol,\alpha}x^k_\alpha S_\alpha)}{\partial t} + \nabla \cdot F^k - \sum_{\alpha\in\{l,g\}} q^k_\alpha = 0, \tag{3-1}$$

where the mass flux of a component is given by:

$$F^k = \sum_{\alpha\in\{l,g\}} (\rho_{mol,\alpha}\upsilon_\alpha x^k_\alpha - D^k_{\alpha,pm}\rho_{mol,\alpha}\nabla x^k_\alpha) \tag{3-2}$$

Here, ϕ represents the porosity and q_α^k represents the source/sink term. $D_{\alpha,pm}^k$ is the macroscopic diffusion constant of component k in the porous media for a multi-phase system. The diffusion coefficient is dependent on the soil properties and the fluid saturation. The phase velocities are described with the extended Darcy's law:

$$v_\alpha = -\frac{k_{r\alpha}}{\mu_\alpha}\mathbf{K}(\nabla P_\alpha - \rho_\alpha g), \quad \alpha \in \{l, g\} \tag{3-3}$$

Combining the equations 3-1, 3-2 and 3-3 described above, we get the mass balance of each component $k \in \{H_2O, CH_4, NaCl\}$, as:

$$\begin{aligned} &\sum_{\alpha\in\{l,g\}} \frac{\partial(\phi\rho_{mol,\alpha}x_\alpha^k S_\alpha)}{\partial t} - \sum_{\alpha\in\{l,g\}} \nabla\cdot\left\{\frac{k_{r\alpha}}{\mu_\alpha}\rho_{mol,\alpha}x_\alpha^k K(\nabla P_\alpha - \rho_\alpha g)\right\} \\ &- \sum_{\alpha\in\{l,g\}} \nabla\cdot(D_{pm,\alpha}^k\rho_{mol,\alpha}\nabla x_\alpha^k) - \sum_{\alpha\in\{l,g\}} q_\alpha^k = 0, \end{aligned} \tag{3-4}$$

where ρ_{mol} is the molar density and μ is the viscosity.

Salt Precipitation

The amount of $NaCl$ precipitated once the salinity of the solution exceeds the solubility product is calculated as follows:

$$q_\alpha^k = \begin{cases} \partial(\phi\rho_{mol,l}S_l(x_l^{NaCl} - x_{l,max}^{NaCl})) & for\ k = NaCl, \alpha = l \\ 0 & else \end{cases} \tag{3-5}$$

Salt Dissolution

The amount of solid $NaCl$ dissolved during washing, when the injection of fresh water reduces the water salinity below the solubility product, is calculated by equation 3-5. The difference is that for dissolution the value of q_l^{NaCl} calculated is negative, while for precipitation it is positive.

Mass Conservation of Precipitated Salt

The mass conservation of the precipitated salt is given by equation 3-6:

$$\frac{\partial(\phi_s^{NaCl}\rho_{mol,s}^{NaCl})}{\partial t} + q_l^{NaCl} = 0 \tag{3-6}$$

The change in porosity of the porous medium, due to this precipitation is given by:

$$\phi = \phi_0 - \phi_s^{NaCl} \tag{3-7}$$

Here, ϕ_s^{NaCl} refers to the solidity or the amount of solid $NaCl$ which was precipitated.

3-1-3 Supplementary constraints

The transport equation (Equation 3-4) has a number of unknowns which have to be solved. There is thus the necessity to introduce certain additional equations in the form of supplementary constraints. The supplementary constraints used in this model are as follows:

1. The pore space is completely occupied by the liquid and gas phases:

$$S_l + S_g = 1 \tag{3-8}$$

2. The pressure of the secondary phase is determined by the capillary pressure, which has been defined by a constitutive relationship (see subsection 3-1-4):

$$p_l = p_g - p_c, \tag{3-9}$$

where p_l and p_g are the liquid and gas phase pressures respectively.

3. The sum of mass or mole fractions of all components $k \in \{H_2O, CH_4, NaCl\}$ present in each phase $\alpha \in \{l, g\}$, equals one:

$$X_l^{H_2O} + X_l^{CH_4} + X_l^{NaCl} = x_l^{H_2O} + x_l^{CH_4} + x_l^{NaCl} = 1 \tag{3-10}$$

$$X_g^{H_2O} + X_g^{CH_4} = x_g^{H_2O} + x_g^{CH_4} = 1 \tag{3-11}$$

4. The density and viscosity of the brine is calculate as a function of its temperature, pressure and salinity, as given in Batzle and Wang [1992]:

$$\begin{aligned}\rho_l =& \rho_{H_2O} + 1000 X_l^{NaCl}\{0.668 + 0.44 X_l^{NaCl} + [300p - 2400 p X_l^{NaCl} + \\ & T(80 - 3T - 3300 X_l^{NaCl} - 13p + 47 p X_l^{NaCl})] \times 10^{-6}\}\end{aligned} \tag{3-12}$$

$$\begin{aligned}\mu_l =& 0.1 + 0.333 X_l^{NaCl} + (1.65 + 91.9 (X_l^{NaCl})^3)\ exp[((0.42 (X_l^{NaCl})^{0.8} - 0.17)^2 \\ & + 0.045) T^{0.8}]\end{aligned} \tag{3-13}$$

5. The salt precipitation model used assumes chemical equilibrium. The different phases are thus in equilibrium with respect to the exchange of components. This is ensured by assuming that the fugacity of each component $k \in \{H_2O, CH_4, NaCl\}$ in each phase $\alpha \in \{l, g\}$ is equal, as discussed by Class et al. [2002], Lauser et al. [2011].

Primary variables

The conservation equations contain several variables that are unknown. Supplementary equations are used to remove some of these unknown variables. The remaining unknown variables are called primary variables and they are computed directly from the iteration steps of the

numerical model. Suitable primary variables have to chosen during modelling. The number of primary variables can be determined according to the Gibbs phase rule.

$$F = k + 1, \tag{3-14}$$

where k represents the number of components present in the model. In equation 3-14, the number of degrees of freedom(F) indicates the required number of primary variables. Secondary variables are determined from the available primary variables. The primary variables and the switching criterion used in the salt precipitation model are shown in table 3-1

Phase State	**Phase Present**	**Primary Variables**	**Switch Criterion**
Gas phase only	Gas	$p_g, x_g^{H_2O}, \phi_l^{NaCl}$	$x_g^{H_2O} > x_{g,max}^{H_2O}$
Liquid phase only	Liquid	$p_l, x_l^{CH_4}, x_l^{NaCl}, \phi_s^{NaCl}$	$x_g^{CH_4} > x_{l,max}^{CH_4}$
Both phases	Gas and Liquid	$p_g, S_l, x_l^{NaCl}, \phi_s^{Nacl}$	$S_{\alpha\in\{l,g\}} = 0$

Table 3-1: Primary variables and switching criterion for different phase presences

3-1-4 Constitutive Relationships

The p_c - S_w Relationship

Constitutive relationships are required to model the discontinuities in pressure across a fluid-solid interface (capillary pressure). Conventional P_c - S_w relationships model the capillary pressure as a function of the effective water saturation and is not defined below the irreducible water saturation. In the case of salt precipitation, due to evaporation, the water saturation in the pores is brought down to below the irreducible saturation (also called apparent residual saturation). A regularized Brooks-Corey approximation of capillary pressure is thus used, which carries out a quadratic extrapolation of the capillary pressure below the irreducible water saturation. The quadratic regularization of P_c, below the apparent residual saturation is shown in Fig. 3-1. Advantages of carrying out regularization are as follows:

- Regularization gives differentiable curves, which is better for the Newton-Raphson scheme.
- Following a "non-regularized" capillary pressure law for small values of liquid saturation, leads to infinite capillary pressure values.

The effective water saturation for a porous medium containing gas and water is defined as follows:

$$S_{we} = \frac{S_w - S_{wr}}{1 - S_{wr} - S_{gr}} \tag{3-15}$$

The Brooks-Corey capillary pressure - saturation relationship Brooks and Corey [1964] is given by:

$$p_c = p_e S_{we}^{\left(-\frac{1}{\lambda}\right)} \tag{3-16}$$

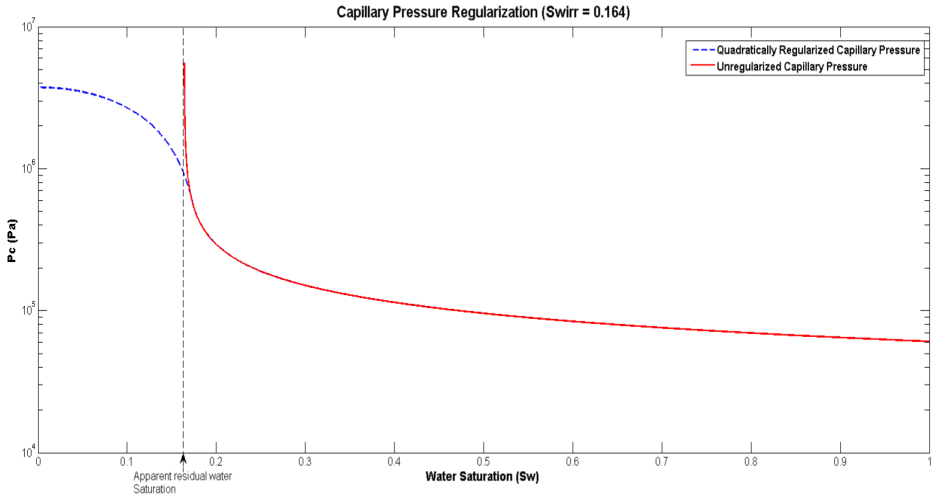

Figure 3-1: Quadratic Regularization of Capillary pressure below the apparent residual saturation

During the precipitation of salt, the porosity and permeability of the rock changes according to the equations 3-7 and 3-20. This change in porosity and permeability causes a change in the entry pressure (p_e) for the capillary pressure. Thus a correction for the capillary pressure must be introduced following precipitation every timestep. This dynamic capillary pressure correction is given by an adaptation of the J-leverett function:

$$p_{ci+1} = p_{ci}\sqrt{\frac{K_0}{K_i} \times \frac{\phi_i}{\phi}}, \tag{3-17}$$

where 'i denotes the current time step.

Furthermore, it was observed that for high capillary entry pressures (P_e) and low water saturations, the capillary pressures can reach values higher than the gas phase pressures. Since $p_l = p_g - p_c$, this results in negative values of liquid phase pressures which are not physical. In order to avoid such unphysical values, the minimum value of the liquid phase pressure was set to be equal to the vapor pressure. The capillary pressure curve was modified accordingly.

The k_r - S_w Relationship

In multiphase flows, the different phases influence the flow properties of each other. This effect is accounted for by introducing a dimensionless parameter 'K_r', the relative permeability. The relative permeability is a function of the wetting phase saturation. The relative permeability of the wetting and non-wetting phases has been determined by the Brooks-Corey model, as a function of the effective saturation and the empirical Brooks-Corey parameter 'λ', as:

$$k_{r,w} = S_{we}^{\frac{2+3\lambda}{\lambda}} \tag{3-18}$$

$$k_{r,n} = (1 - S_{we})^2 \left(1 - S_{we}^{\frac{2+\lambda}{\lambda}}\right) \tag{3-19}$$

According to Yiotis et al. [2004] and others, capillary film flow is present below the irreducible liquid saturation. In order to model film flow, the corner flow model was developed by Mahadevan et al. [2006]. This model gives a quadratic regularization of the liquid relative permeability below the apparent residual. In this work, a quadratic regularization of the liquid relative permeability has been carried out, to depict the effect of capillary film flows on the salt precipitation profile (Fig. 3-2).

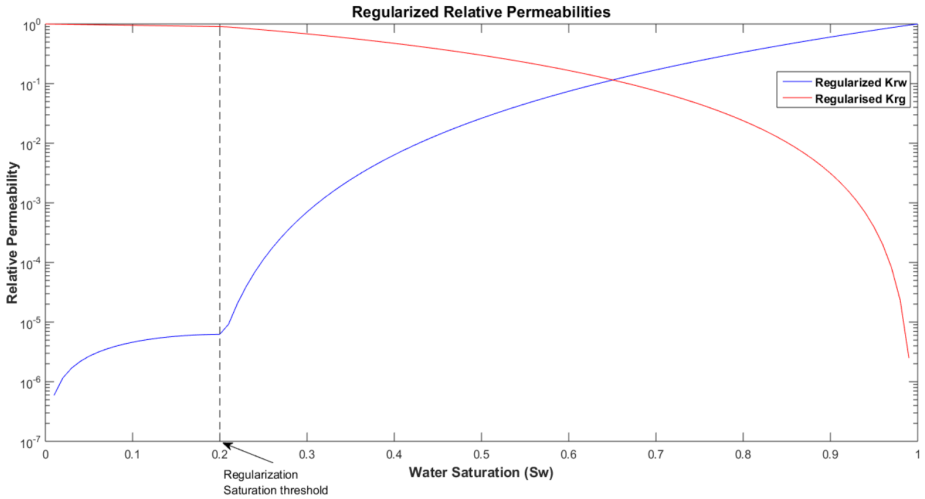

Figure 3-2: Regularization of relative permeabilities below the apparent residual saturation

The Porosity - Permeability Relationship

Different porosity-permeability relations are found to be depictive of different soil types. In the salt precipitation model, three different relationships, namely the Kozeny-Carmen, The Verma-Pruess and the Power Law relationship have been implemented. The Power Law was found to be the best fit with field data and is being used to calculate the changes in permeability, due to changes in porosity. The power law is as follows:

$$\frac{K}{K_0} = \left(\frac{\phi}{\phi_0}\right)^n, \tag{3-20}$$

where 'n' is an exponent which was found to be approximately 15, through curve fitting of the field data.

3-2 Spatial Discretization

In this model, the spatial discretization of the domain is carried out by DuMu^X, using the BOX method. "The BOX method unites the advantages of the finite-volume(FV) and the finite-element(FE) methods" Leh [2014]. A short introduction to the Box method, as given in Leh [2014], is described in appendix A-1.

3-2-1 Reservoir Simulation Model

A radial symmetric model has been used to investigate near-wellbore salt deposition in DuMu^X. The base case radial symmetric model is shown in figure 3-3a. In order to reduce computational time, a piece of the radial symmetric model was used in all the simulations (see Fig. 3-3b. It was verified earlier that the results obtained from the radial symmetric model coincided with the results obtained from the piece of the radial model. It can be observed from figures 3-3a and 3-3b, that the grid sizes increase gradually on moving away from the wellbore. This has been carried out to reduce computational time, since the salt deposition phenomenon has been found out to be predominantly a near-wellbore issue. The phenomenon thus requires greater definition near the wellbore, when compared to locations some distance away from the wellbore.

The inner and outer reservoir boundary are set up using a dirichlet condition, while the other faces of the model have a no flow neumann boundary.

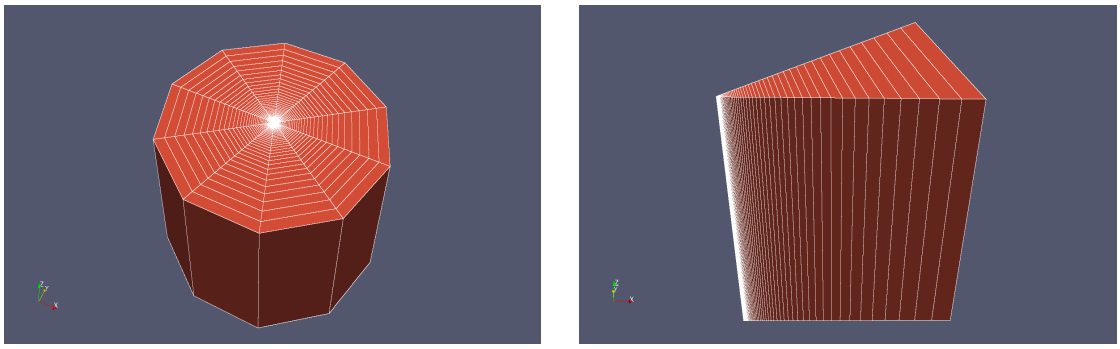

(a) Radial Symmetric Model

(b) Piece of the Radial Symmetric Model

Figure 3-3: Simulation Models

3-2-2 Grid Refinement Study

A grid refinement study was carried out on the radial symmetric model, to choose the optimum grid size which can describe the near and away from wellbore salt precipitation, while easing simulation time and maintaining a certain accuracy.

Generally, coarse grids better the computational speed, but compromise on accuracy. On the contrary, fine grids provide better accuracy, but are computationally time intensive. We therefore need to find a compromise between accuracy and computational cost.

The results of the grid refinement study can be seen in 3-4 for near wellbore salt precipitation and in Fig. 3-5 for away from wellbore precipitation. Figures 3-4 and 3-5 suggests that a grid size which is four times smaller than the initial grid size used, is ideal for the purposes of modelling salt precipitation. The piece of the radial model, which was utilized for all further simulations, is shown in Fig. 3-6.

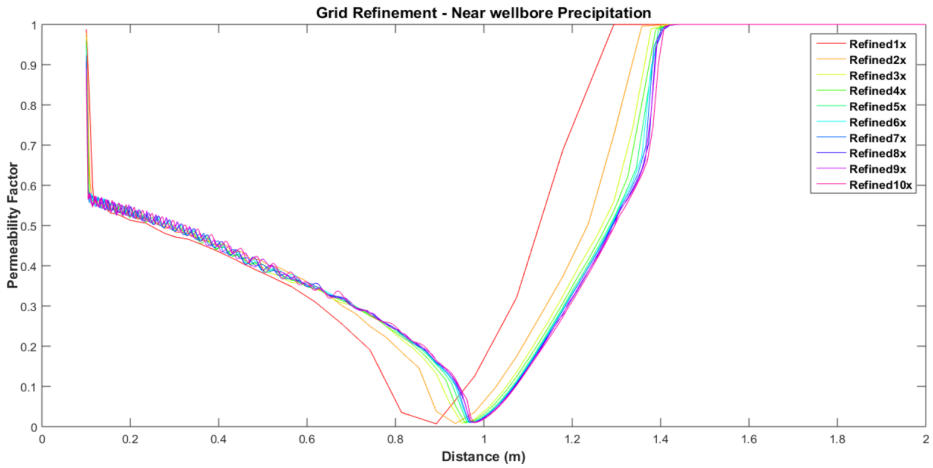

Figure 3-4: Grid refinement study for near-wellbore precipitation

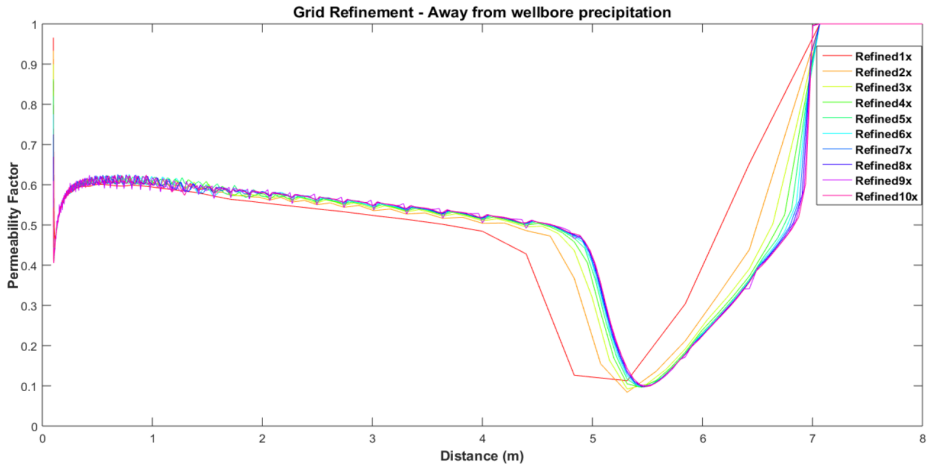

Figure 3-5: Grid refinement study for away from wellbore precipitation

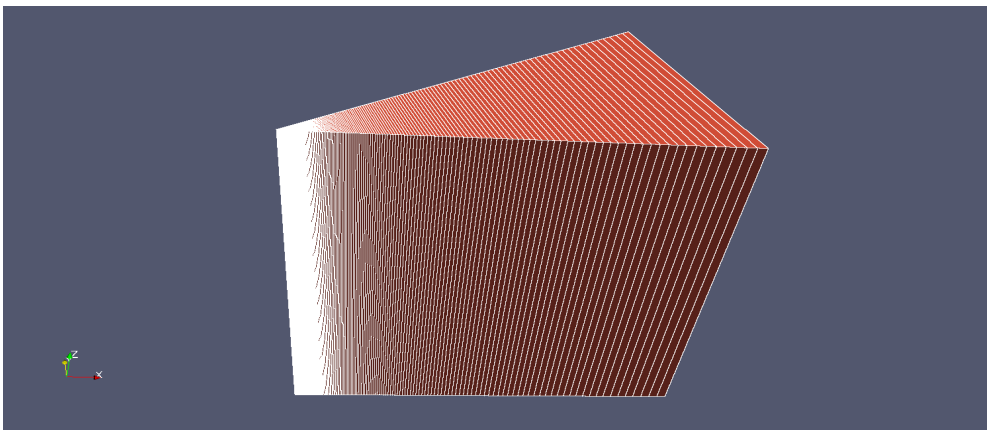

Figure 3-6: The 4x refined model used for all further simulations

3-3 Time Discretization

The fully implicit Euler scheme is used to carry out the temporal discretization in this model Pavuluri [2014]. This means that the simulator solves the equations for variables at an unknown time step (t_{i+1}), by referring to the variables at a known time step (t_i). The time derivatives present in the storage term of the mass balance equation can be described as follows:

$$\frac{\partial x}{\partial t} = \frac{x^{i+1} - x^i}{t_{i+1} - t_i} = A^{i+1} x^{i+1}, \tag{3-21}$$

where x^{i+1} denotes the vector containing unknown variables at the new time step t_{i+1}; x^i, the unknown variables at the previous time step t_i and A^{i+1} is the coefficient matrix for the new time step. The fully implicit scheme is very advantageous, since it is highly stable and there is no restriction in choosing large time step sizes. However, large time steps can result in a loss of accuracy of the solution.

3-4 Benchmark: DuMu^X - Tough2

The salt precipitation model implemented in DuMu^X was benchmarked with another numerical simulator called Tough2 Egberts [2014] and in some cases additionally with a semi-analytical tool(AEM) developed by TNO, for a specific set of input parameters.This was done due to the absence of experimental measurements of salt precipitation in sandstone cores. The benchmarking process was carried out in five stages:

1. Effect of evaporation on water saturation (Fig. 3-7a).
2. Evaporation of saline water
3. Evaporation of saline water with resulting permeability reduction due to precipitation
4. Effect of combined darcy flow and evaporation of saline water with permeability reduction (Fig. 3-8).
5. Evaporation of saline water with salinity dependent vapor pressure lowering

The benchmark results(Fig. 3-7 and 3-8), show that there is a very good agreement between the numerical simulators for modelling evaporation and a reasonable match for modelling salt precipitation.

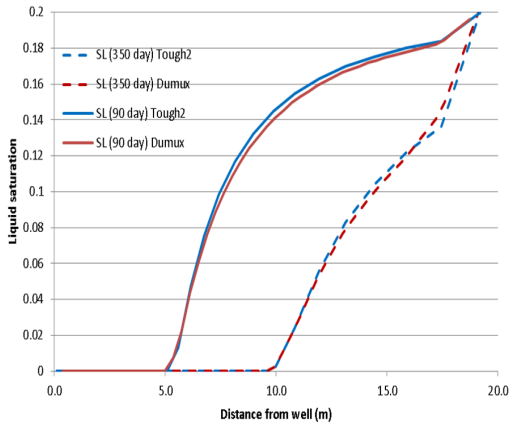

(a) Effect of evaporation on water saturation

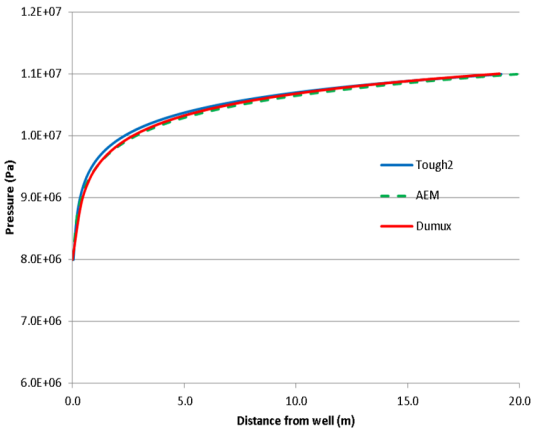

(b) Effect of evaporation on the steady state pressure profile

Figure 3-7: Benchmark: Impact of Evaporation (from Egberts [2014])

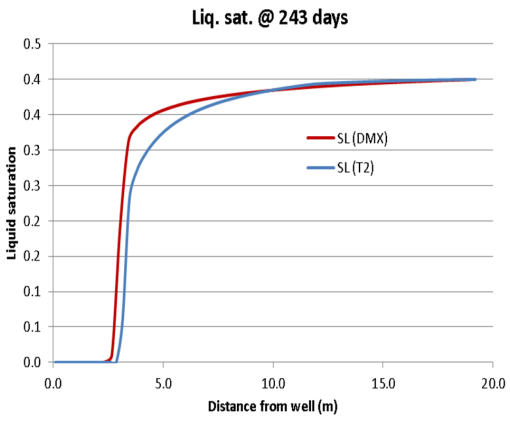

(a) Effect of darcy flow, evaporation and precipitation on the water saturation

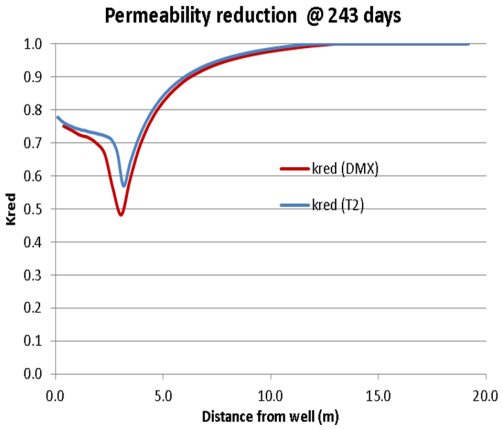

(b) Effect of precipitation on the permeability factor

Figure 3-8: Benchmark: Combined Model -Impact of darcy flow, evaporation and precipitation(from Egberts [2014])

Chapter 4

Results and Discussions

In this chapter, the concept of a balance between the rate of drying and rate of precipitation in a reservoir is introduced. Furthermore, a sensitivity analysis is carried out to measure the impact of changing some crucial parameters, on the salt precipitation profile. The drying-transport balance hypothesis is then used to interpret and explain the different salt precipitation profiles being observed during the sensitivity analysis.

4-1 The Drying - Transport Balance Hypothesis

In this section, the concept of a drying-transport-balance is introduced to explain the location and timescale of salt precipitation.

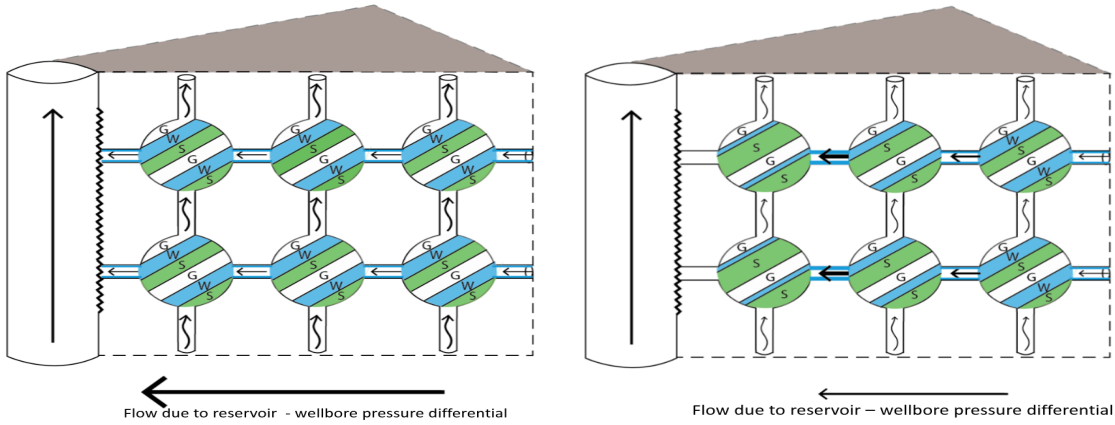

(a) Initial state of the reservoir during gas production

(b) Capillary flow due to drying

Figure 4-1: Pore network graphic - The salt precipitation phenomenon

Fig. 4-1 shows a pore network graphic, which gives a visual representation of the different physics involved in the salt precipitation phenomenon. Arrows shown in bold, indicates that

the particular phenomenon it is referring to is prominent. The curly arrows depicts drying due to evaporation, while the horizontal arrows placed in the pore throats indicate flow due to capillary pressure differential. The segmented representation of gas, water and salt in the pores, is done to give a REV (Representative Elementary Volume) style representation. Fig. 4-1a depicts an initial state of the reservoir during gas production, while Fig. 4-1b depicts a state wherein some drying has already taken place and capillarity controls the liquid transport in the pores.

Initially,the liquid flow due to reservoir - wellbore pressure differential is very high. As the liquid saturation in the region near the wellbore drops and goes below the irreducible saturation, the liquid production ceases. Since the liquid saturation is initially almost the same throughout the reservoir, the rate of liquid transport through capillary pressure differential is relatively low.

In Fig. 4-1b, it can be observed that that the pores near the wellbore have reduced water saturations, due to drying as a result of gas expansion (see section 2-2). This results in a higher rate of capillary driven liquid transport. Additionally, It can be seen that the amount of salt precipitated has increased in these pores as a result of drying. This causes a pressure drop due to salt skin and thus reduces the rate of evaporation. The drying transport balance occurs when the rate of capillary driven liquid transport is slightly higher than the rate of removal of water from the pores due to evaporation.

4-1-1 Parameters Influencing Drying

Some of the different parameters influencing the rate of drying are:

1. **Reservoir pressure differential:** The amount of water evaporating into the gas phase during flow-through drying, due to flow of a saturated gas, depends on the amount of gas expansion taking place. The gas expansion in turn depends on the pressure differential in the reservoir. A large pressure differential leads to expansion in the gas phase and therefore increases the rate of drying.
2. **Capillary pressure:** Flow due to capillary pressure differential results in the movement of water from a zone with a lower rate of drying to a zone with a higher rate of drying. This leads to an overall increase in the rate of drying. Higher the capillary pressure, higher the rate of drying.
3. **Salinity:** The saturation vapor pressure of the gas depends on the salinity of the formation water, due to the phenomenon of vapor pressure lowering. This means that the amount of water vapor present in the gas at a point of time depends on the salinity of the formation water. A higher amount of dissolved salts results in a lowered rate of drying.
4. **Solubility Limit:** The solubility limit of salt in water decides the limit to which the salinity of water can increase before salt starts precipitating out of the solution.

4-1-2 Parameters Influencing Liquid Transport

Some of the different parameters influencing the rate of liquid transport are:

1. **Water Relative Permeability:** The water relative permeability affects the rate of liquid transport, since they affect the mobility of liquid. The relative permeability curves are specific to each geological formation.

2. **Water saturation:** The water saturation is an important parameter for deciding the rate of liquid transport. A high value of water saturation results in a high value for the liquid relative permeability and in turn a higher rate of liquid transport.

3. **Capillary Pressure:** A high capillary pressure results in lower water phase pressures, since for a reservoir containing only gas and water, $p_c = p_g - p_w$. This difference in water phase pressure causes capillary flow of water to the drying zone.

4. **Irreducible saturation:** The value of irreducible saturation marks the water saturation below which the formation water stops flowing. The irreducible saturation is an input parameter for the salt precipitation model. In case regularized relative permeability curves are used in the model, this value marks the transition of the flow regime into one of capillary film flow.

5. **Salinity:** The density and viscosity of the formation water depends on its salinity. Therefore the salinity thus affects the mobility of the liquid and in turn influences the rate of liquid transport.

4-1-3 Proof of Drying - Transport Balance

It has been observed in most of the simulations where the initial rate of drying is high, that the location of salt precipitation keeps moving away from the wellbore with time. This happens until at one point of time the salt keeps precipitating in one location. It is at this point of time, that the reservoir has achieved a drying-transport balance.

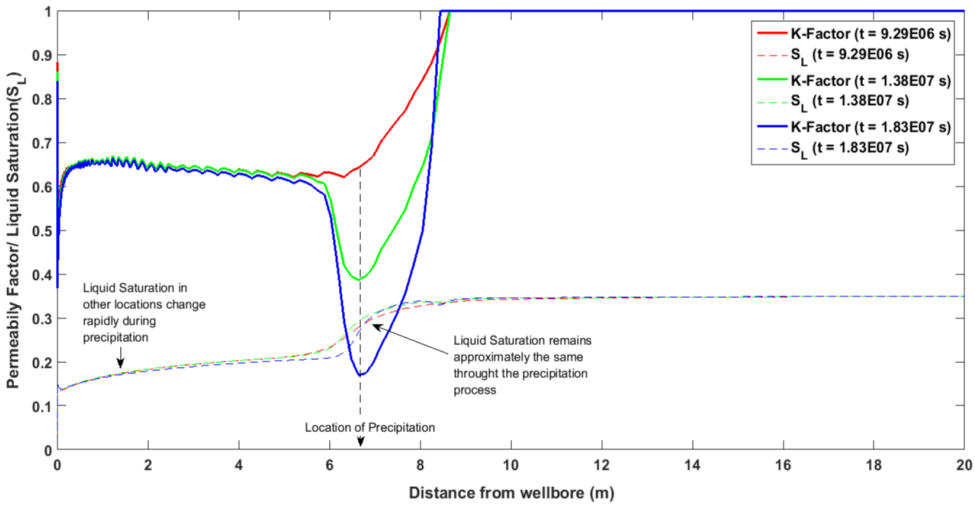

Figure 4-2: Figure showing proof of the drying-transport balance

Fig. 4-2 shows a situation where the K-Factor has reduced from a value of 0.75 to a value of 0.17 over the course of approximately 105 days, at the location of the salt precipitation peak

that is seen to be developing. It can be observed that the liquid saturation remains almost constant at that location throughout the precipitation process. The slight changes in liquid saturation that can be observed at the location of precipitation is due to the dynamic capillary pressure corrections occurring due to the reducing permeability, as given by equation 3-17. Furthermore, it can also be noticed that the liquid saturation near the wellbore has reduced from a value of 0.35 to almost 0.15, during precipitation.

This is only possible if there is a balance between the rate liquid loss due to drying and liquid influx due to capillary transport at the precipitation location within the reservoir. Furthermore, the picture depicted in Fig. 4-2 is observable in most of the simulations where there is complete clogging of the pore throats.

To be more accurate about the balance described in the previous paragraph, a volume balance is carried out at the pore scale. Consider a pore, containing some water, gas and dissolved salt, exactly like the DuMu^X salt precipitation model. The dissolution of gas in water is neglected. Initially the volume of liquid in a pore is $V_l^{H_20} + V_l^{NaCl}$. After the volume V_l^{NaCl} of salt has precipitated, the volume of water is now $V_l^{H_2O} + V_t - V_e$, where V_e is the volume of water evaporated and V_t is the amount of liquid transported to the pore due to capillary pressure differential arising due to evaporation. When salt is precipitated, the pore volume reduces by the volume of salt precipitated. Therefore the new pore volume is now $V_{p,new} = V_p - V_l^{NaCl}$ (assuming the volume of dissolved salt going out of solution is equal to the volume of solid salt precipitated).

As shown in Fig. 4-2, it has been observed that the water saturation remains constant during the drying-transport balance. Now, $S_l = \frac{V_l}{V_p}$, and since $S_{l,new} = S_{l,old}$,

$$V_t - V_e = (\frac{V_p - V_l^{NaCl}}{V_p})[V_l^{H_2O} + V_l^{NaCl}] \tag{4-1}$$

Equation 4-1 states the condition necessary to achieve the drying transport balance.

4-1-4 Interpretation of the Halite Precipitation Profile

There are a few observation which can be made about the salt saturation profile based on different simulations. These observations can be used in general for interpreting the salt precipitation profile, both in time and in space. It has also been observed that these physical phenomenon have a dependence on each other. i.e the formation of one condition leads to the formation of another condition. A sequence of conditions which have been observed in multiple simulations, leading to salt clogging and can help interpret the salt precipitation profile, is given below.

1. In the initial stages of production, the liquid phase gets produced for a short period of time through immiscible displacement, before the evaporation regime sets in. Liquid transport then happens only due to the presence of a capillary pressure differential.

2. The drying rate of the liquid phase in the porous medium depends mainly on the gas expansion occurring in the reservoir, due to the pressure differential between the external boundary and the wellbore (see Fig. 4-3). This is because the gas present in

the reservoir is already saturated and need to expand in order to be able to evaporate more liquid. Therefore, a higher reservoir pressure differential leads to a higher rate of drying.

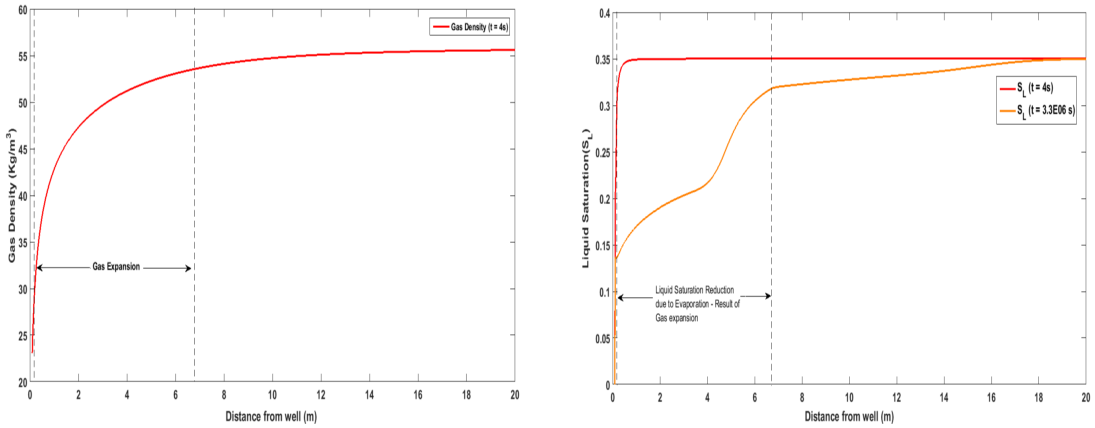

(a) Initial gas density

(b) Comparison of liquid saturation in time

Figure 4-3: Liquid evaporation due to gas expansion

3. A higher rate of drying implies that the solubility limit will be reached earlier. Thus salt is precipitated initially in a reservoir with a higher rate of drying when compared to a reservoir with a lower drying rate.

4. Since the liquid transport is now almost entirely dependent on the capillary pressure differential, a higher rate of drying causes the capillary pressure to be the larger, by causing a bigger reduction in the liquid saturation. This increase in capillary pressure in turn results in a liquid phase pressure differential in the drying zone, which prompts liquid transport (and salt transport) to the drying zone.

5. Depending on the initial values of the p_r, BHP, S_w and salinity, the reservoir can initially be in a drying dominated regime, a transport dominated regime or in a drying-transport balance. A drying or a transport dominated regime means that the rate of drying or transport is respectively higher than the other.

6. In a drying dominated regime, the formation water surrounding the wellbore reaches the solubility limit and the drying starts spreading outwards away from the wellbore, since the liquid transport is not strong enough to supply enough liquid and salt to the drying region (see Fig. 4-4).

7. The precipitated salt creates a pressure drop due to the partial clogging of the pore throats. This creates a reduction in the pressure differential between the external boundary and the drying zone. As mentioned before, a reduced pressure differential implies a lower rate of drying. Therefore in a drying dominated regime, the salt will precipitate till the regime transitions from a drying dominated one to one in which there is a balance between the drying and transport rates. Achieving the drying-transport balance results in salt precipitation being localized within the same region and quick salt clogging.

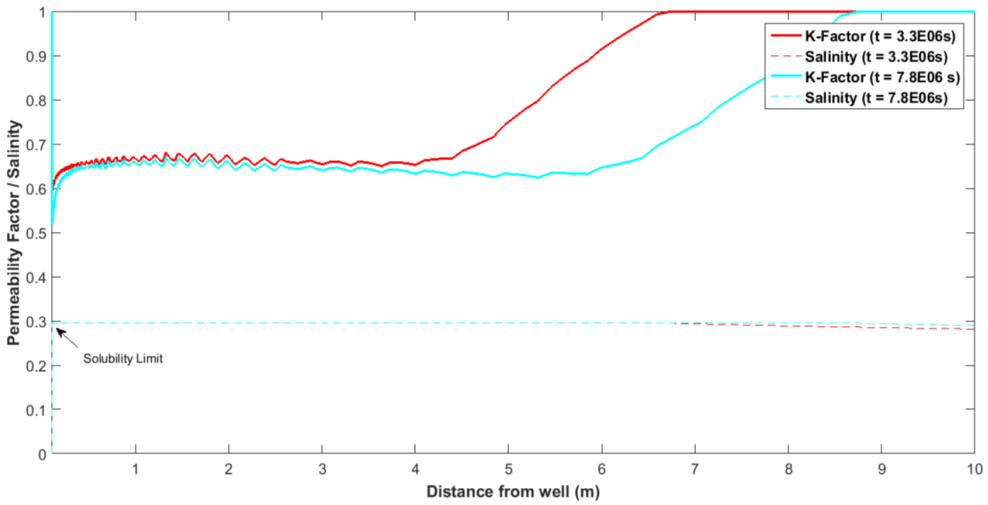

Figure 4-4: Spreading of the drying zone away from the wellbore in a drying dominated regime

8. In a liquid transport dominated regime, a small increase in capillary pressure due to drying results in a movement of liquid to the drying region. The magnitude of liquid transport depends on the liquid phase pressure differential. Since the liquid phase pressure differential keeps increasing with reduction in liquid saturation, there will always come an instance where there is a balance in the rates of drying and transport. Once this drying-transport balance is achieved, the location of salt precipitation remains constant and leads to quick salt clogging. Fig. 4-5 depicts the typical salt precipitation profile in a liquid transport dominated regime. It is observable that the precipitation is very close to the well and that the reduction of liquid saturation near the wellbore is negligible. This signifies that liquid transport counters the effect of drying on the liquid saturation.

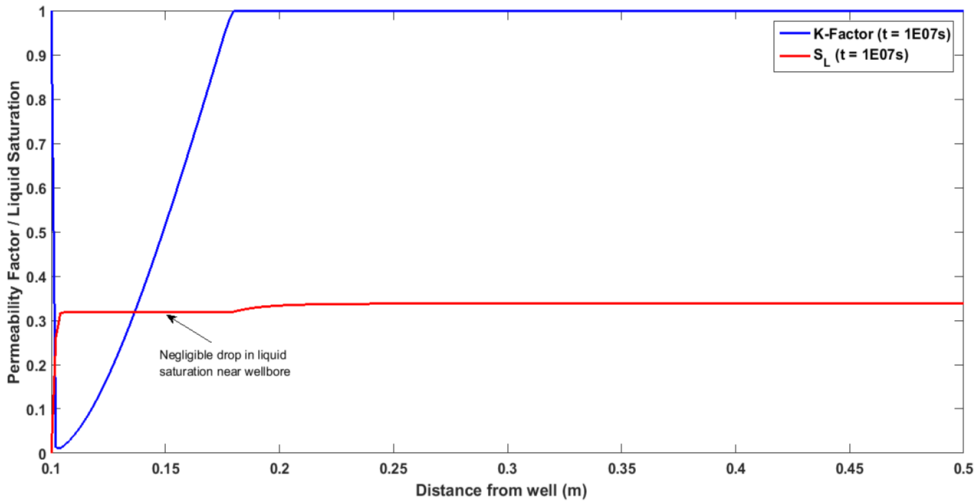

Figure 4-5: Salt precipitation profile in a Liquid transport dominated regime

It is thus easy to interpret the salt precipitation profiles based on the aforementioned observation. A salt precipitation profile with clogging a few meters from the wellbore indicates that the reservoir was initially in a drying dominated regime. A profile with salt clogging very close to the wellbore indicates that the reservoir was either initially in a liquid transport dominated regime or in a balance between the rates of drying and transport.

In the absence of a drying-transport balance, the drying zone doesn't get enough transport of water and salt. The drying zone thus ends up getting partially clogged and having zero liquid saturation, since neighbouring areas will also be at a saturation below the irreducible. Under the assumption of capillary film flow below the apparent residual, the drying-transport balance is not a necessity for achieving salt clogging, since there will be some transport of water and salt to the drying zone in the form of liquid films, even if the neighbouring regions are almost completely dry.

4-2 Sensitivity Analysis and Interpretation

Sensitivity analysis is a study of the sensitivity of a model to changes in the values of parameters inputted to the model and also to changes in the structure of the model. In this section we focus on parameter sensitivity. Parameter sensitivity is carried out by performing a series of tests in which different parameter values are inputted into the model iteratively to observe the change caused in the simulation objective due to a change in the input parameter.

The salt precipitation model has been observed to be very sensitive to changes in certain parameters. Moreover, some parameters change with time in the 'real world'. A sensitivity analysis of these parameters can thus be used to describe how these real world changes can affect the simulation objective. Furthermore, some parameters are very difficult to measure with a good level of accuracy. The sensitivity analysis can thus also be used to estimate the effect of uncertainties in the measurement of these parameters.

Equation 3-20 describes the change in permeability occurring due to a change in the porosity. The term 'K-factor' or 'Permeability Factor' is the fraction $\frac{K}{K_0}$ and represents the reduction in permeability of the representative grid block. A k-factor of zero describes a state wherein the pore throats are completely plugged and gas production takes place no longer. In this work, the K-factor is used in lieu of other parameters like salt saturation to compare the effect of the sensitivity analysis, since it gives a better representation of the impact of precipitation on the gas production.

The subsections 4-2-1 through to 4-2-6 shows the sensitivity of the salt precipitation model to certain critical parameters and their interpretations according to the drying-transport balance hypothesis. The input file giving the parameter values used as a base case for these sensitivity analyses is displayed in appendix A-3

4-2-1 Sensitivity to Initial Permeability

The absolute permeability of a reservoir is a parameter which cannot be estimated with a high level of accuracy, since rocks are usually very heterogeneous and anisotropic with respect to their permeabilities. It is thus important to find out the sensitivity of the model to changes in the absolute permeability.

It can be observed from Fig. 4-6 that the initial permeability of the reservoir rock has a big impact on the salt precipitation profile with respect to the time taken to achieve salt clogging. The effect of changing initial permeabilities on the location of salt precipitation can be described to be more moderate.

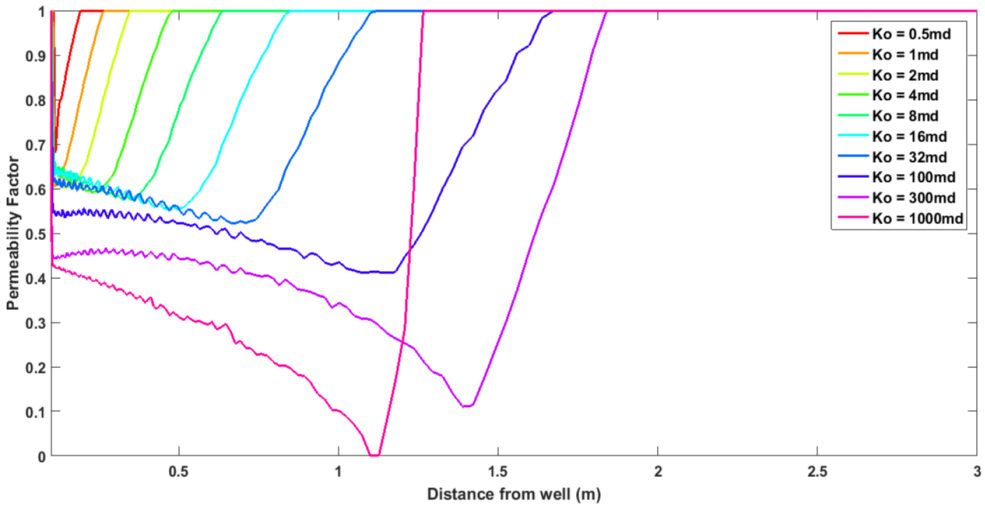

Figure 4-6: Initial permeability sensitivity - Comparison of permeability factors (Time = 212083 s)

In Fig. 4-6, it is seen that the more permeable reservoirs get clogged with salt earlier when compared to reservoirs with lesser initial permeabilities. Furthermore, It can be seen that initially the gas phase pressure differential from the external boundary, till a distance of approximately $1m$ from the wellbore is much higher for the higher permeabilities when compared to the lower permeabilities (Fig. 4-7a). A high pressure differential implies a large expansion in gas volume and as described in section 2-2, gas expansion is directly proportional to the rate of drying in porous media. Therefore it can be said that initially the higher permeability reservoirs have a higher rate of drying. This leads to the the solubility limit being reached the quickest in the most permeable reservoir. This high initial rate of drying causes the gridblocks slightly away from the wellbore to reach their solubility limit and is what causes the location of precipitation to move farther away from the wellbore (rate of drying higher than rate of transport).

However this trend in the gas phase pressures doesn't remain the same for a long period of time, the trend reverses after salt precipitation. Fig. 4-7b depicts the gas phase pressures after some salt has been deposited. Salt deposition is akin to the development of skin in the sense that it impairs the productivity of a well by creating a pressure drop near the wellbore. Once salt starts getting precipitated, the gas phase pressure differential from the reservoir boundary to the drying location decreases for the higher permeabilities. This results in a decrease in the rate of drying. Since the rate of drying was high for a period of time, the water saturation in the high permeability case is much lower than the less permeable cases. This results in a higher capillary pressures (see Fig. 4-8) for the higher permeabilities and consequently higher water phase pressure differentials. This in turn leads to a higher rate of transport.

It is this combined effect of low drying and higher transport rates in the later stages for the

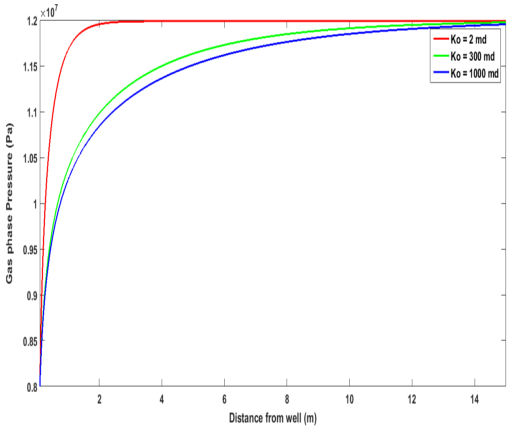

(a) Initial gas phase pressures (Time = 4.5 s)

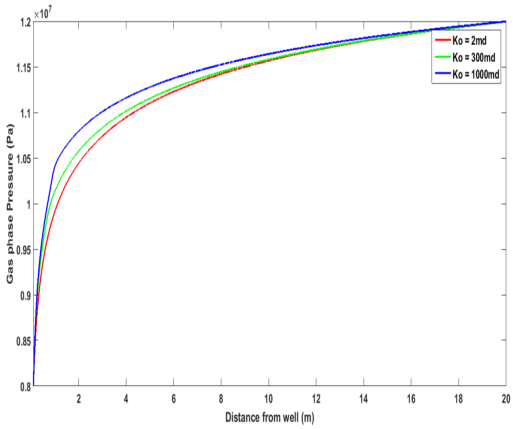

(b) Gas phase pressures later in time (Time = 17307.6 s)

Figure 4-7: Comparison of gas phase pressures

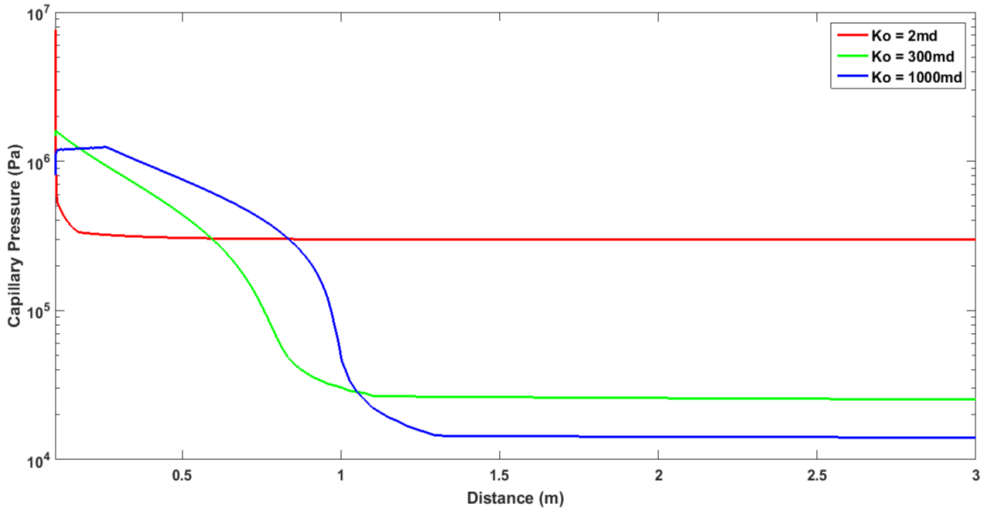

Figure 4-8: Comparison of capillary pressures

higher permeability rocks that causes the drying-transport balance to be achieved the quickest in them. This drying-transport balance in turn results in the more permeable rocks getting clogged with salt earlier.

4-2-2 Sensitivity to the Reservoir Pressure

In the 'real world', the reservoir pressure is a parameter which declines continuously with maturation of the reservoir. It is therefore important to understand the sensitivity of the model with respect to the reservoir pressure. The sensitivity analysis of the model towards the reservoir pressures has been carried out by conducting multiple DuMu^X simulations, wherein the BHP is kept constant at 80 bar and the reservoir pressure is varied between 85 bar and 170 bar.

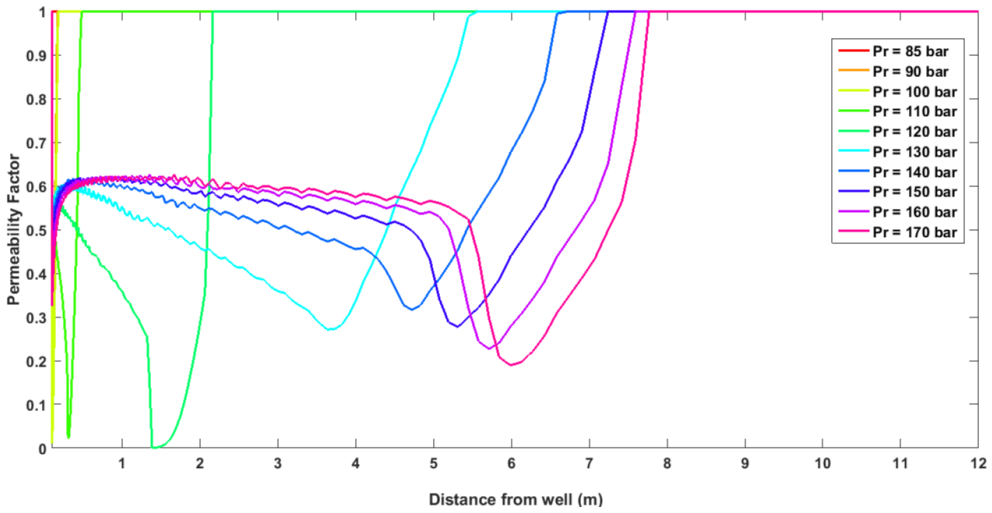

Figure 4-9: Reservoir pressure sensitivity - Comparison of permeability factors (Time = 1.233E07) (BHP = 80 bar)

It can be observed from Fig. 4-9 that the salt precipitation model is very sensitive to changes in reservoir pressure, both spatially and in time. The sensitivity of the K-factor to the change in reservoir pressure is not monotonic. It can be seen that the lower reservoir pressures clog earlier and closer to the wellbore. Furthermore, it can be observed that the higher reservoir pressures clog earlier when compared to the moderate reservoir pressures. In the figure, the reservoir pressure of 140 bar is found to clog the latest in time. This provides proof that there is an optimum value of drawdown in each reservoir, which when maintained can delay salt clogging. Moreover, it shows that producing at the highest drawdown may not be the best strategy for wells having the salt precipitation issue.

The K-factor profile shown in Fig. 4-9 can be interpreted based on the drying-transport balance hypothesis. As discussed in subsection 4-2-1, reservoir pressures smaller than 130 bar have a low rate of drying due to limited gas expansion. The time taken for these reservoirs to attain the drying-transport balance is thus shorter than the higher reservoir pressures. This leads to a quicker clogging of the pore throats with salt.

The question then arises why the highest drawdowns are also having a low K-Factor in the same timestep. Intuitively, the higher reservoir pressures are expected to have a higher rate of drying and thus they should be taking progressively longer times to reach the drying transport balance and also to get clogged. This can be answered by looking at Fig. 4-10. It can be seen that the higher reservoir pressures initially have a higher rate of drying and due to the reduction in water saturation due to drying, they develop a large capillary pressure differential. The higher reservoir pressures thus attain the drying-transport balance at a higher rate of drying and water transport when compared to the lower reservoir pressures. This ensures that the rate of precipitation of salt and consequently the reduction in K-factor is the quickest for the higher reservoir pressures.

The sensitivity of the location of salt precipitation with respect to the reservoir pressures is quite intuitive, with the higher reservoir pressures precipitating salt farther away from the wellbore. This is a point of concern, when looking at the amount of water required for dissolving the salt precipitated, up to a few meters away from the well. An additional point of

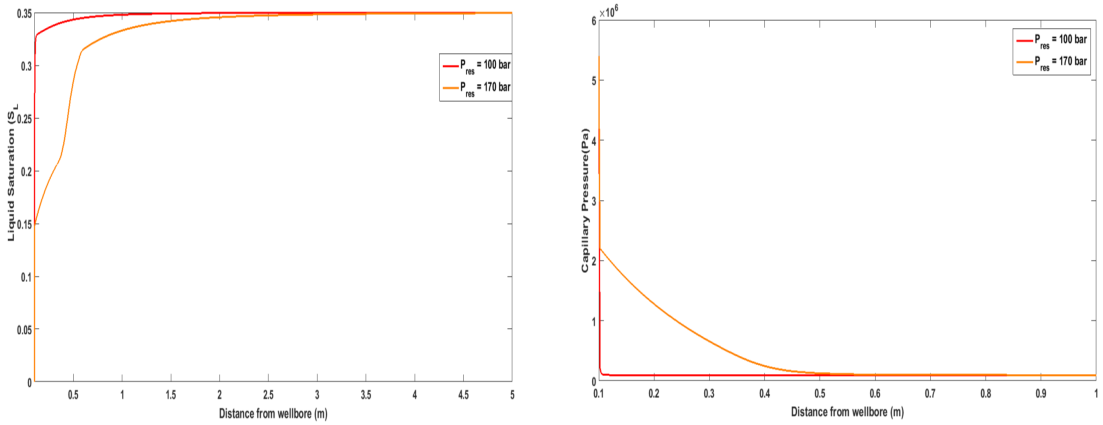

(a) A comparison of liquid saturations showing the relative rates of drying

(b) Comparison of capillary pressures evolved due to different drying rates

Figure 4-10: Comparison of liquid saturation and Capillary pressures for different reservoir pressures

concern is the possibility of formation of water blocks Mahadevan and Sharma [2005], during flow back of the injected water. A study on the amount of water required to wash the salt precipitated and the possibility of formation of water blocks and their dissipation can lead to new conclusion regarding the optimum reservoir management strategy for maximizing the cash flow.

4-2-3 Sensitivity to Irreducible Water Saturation

The irreducible water saturation of a rock is an important parameter which determines the relative permeabilities and capillary pressures associated with different values of water saturation. Therefore, any change in this parameter introduces a change to the rate of transport of water.

Fig. 4-11 depicts the sensitivity of the K-factor to various values of irreducible saturation. It can be observed that when the irreducible saturation values are high, there is very little precipitation and the location of precipitation tends to move away from the wellbore. However, when the S_{wirr} values are low, the K-factors are nearly zero and the location of salt precipitation is right next to the wellbore (Fig. 4-11b).

As mentioned before, a change in the S_{wirr} changes the capillary pressures and liquid relative permeability attributed to a specific value of saturation. Therefore these trends can be explained with the help of a comparison of water mobilities, as shown in Fig. 4-12. it can be seen that a lower value of S_{wirr} corresponds to much higher value of water mobility. On the contrary, the capillary pressures will be higher for a higher value of irreducible saturation. This is because the asymptote of the capillary pressure curve (see Fig. 3-1 is realized for a higher value of water saturation. However, these higher values of capillary pressure don't contribute to liquid transport, since the water saturations quickly recede below the irreducible limit. Therefore, the water mobility describes the liquid transport to a large extent. These high mobilities result in a high rate of water transport, which fulfills the conditions required

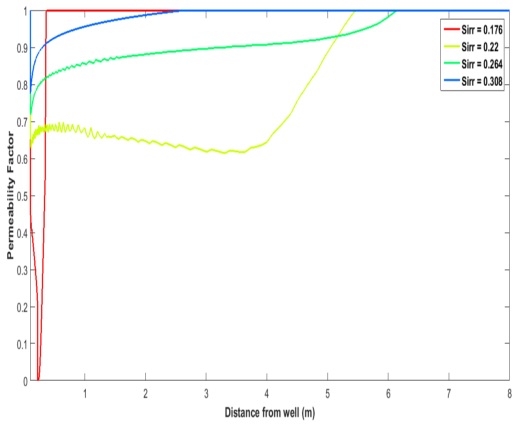

(a) Irreducible water saturation sensitivity - High S_{wirr} (Time = 1E07 s)

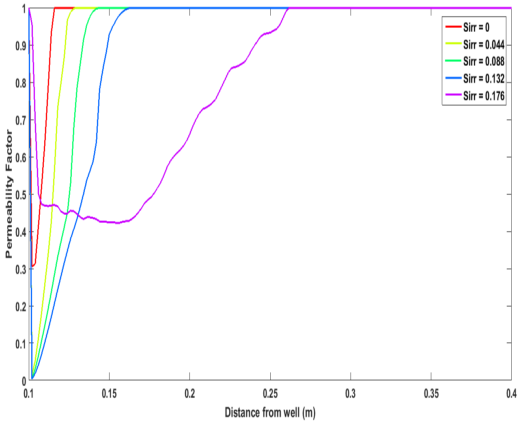

(b) Irreducible water saturation sensitivity - Low S_{wirr} (Time = 6889.3 s)

Figure 4-11: Irreducible water saturation sensitivity - K-Factor comparison

for the drying-transport balance and leads to quick and near to the wellbore precipitation.

The trends shown in Fig. 4-11b are indicative of the fact that including the effect of film flow in the salt precipitation model can give rise to salt precipitation very close to the wellbore. Moreover, this is analogous to the observations made by the operators of gas fields plagued by salt precipitation.

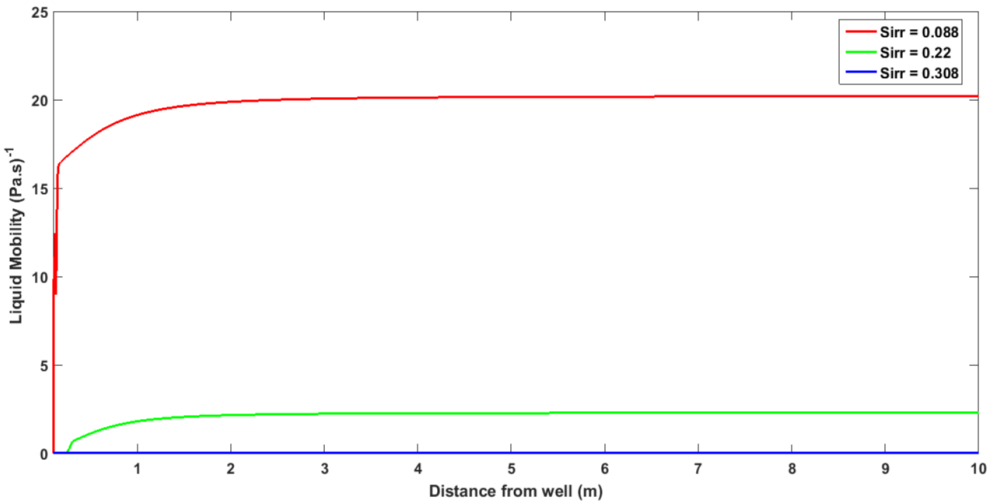

Figure 4-12: Comparison of liquid mobilities

The low rate of precipitation of sirr=0 (Fig. 4-11b), when compared to the other low saturations can be attributed to the fact that in this model, the capillary pressure curve is capped by ensuring the liquid phase pressure does not reduce below the vapor pressure (see section 3-1-4).

4-2-4 Sensitivity to Initial Water Saturation

The salt precipitation model was found to be extremely sensitive to small changes in the value of initial water saturation. The sensitivity of the salt precipitation model to changes in the water saturation is displayed in Fig. 4-13

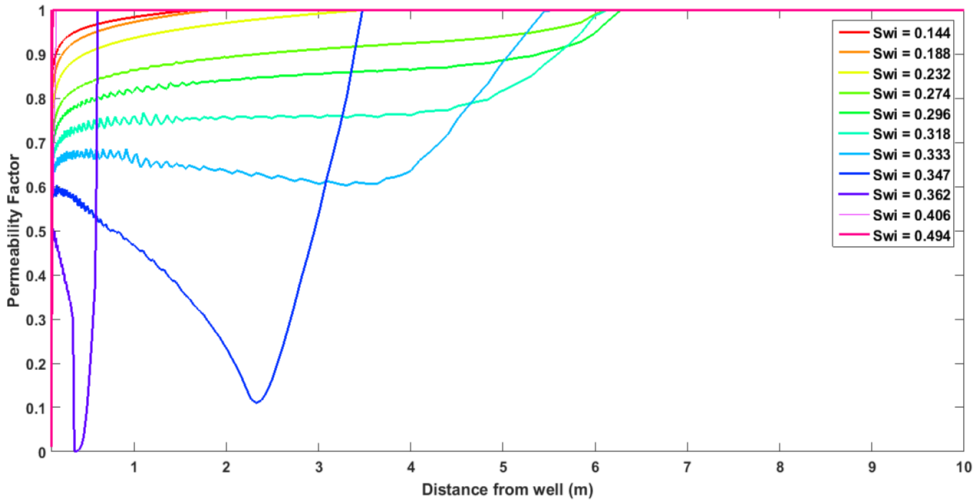

Figure 4-13: Initial water saturation sensitivity - Comparison of permeability factors (Time = 1E07 s)

The trends observed in Fig. 4-13 are very similar to the trends observed in subsection 4-2-3, with the sensitivity of the model to S_{wirr}. A high value of S_{wi} results in salt precipitation very close to the wellbore. However, the salt is not precipitated earlier for higher water saturations. A low value of water saturation results in salt precipitation away from the wellbore and in smaller concentrations. The value of S_{wirr} taken for all these simulations is 0.2.

The sensitivity of the model w.r.t the S_{wi} can be explained on the basis of varying rates of water transport. A high value of water saturation corresponds to high water relative permeabilities and consequently high water mobilities. Therefore even a small reduction in water saturation due to drying, will be compensated by water transport from neighbouring areas. This implies a continuous transport of salt to the near wellbore areas. Furthermore, since in a radial symmetric model, the volume of the area near the well is the minimum, the pore volume near the wellbore is thus also the least and this leads to pore clogging with minimal precipitation of salt.

4-2-5 Sensitivity to Initial Water Salinity

Salinity has been found to be a very critical parameter in the salt precipitation model. Furthermore, determination of the formation water salinity can be quite uncertain. The following are the parameters affected by salinity:

- Density of formation water
- Viscosity of formation water

- Rate of evaporation, through lowering of the vapor pressure

Therefore it is important to see the dependence of the salt precipitation model to changes in the salinity.

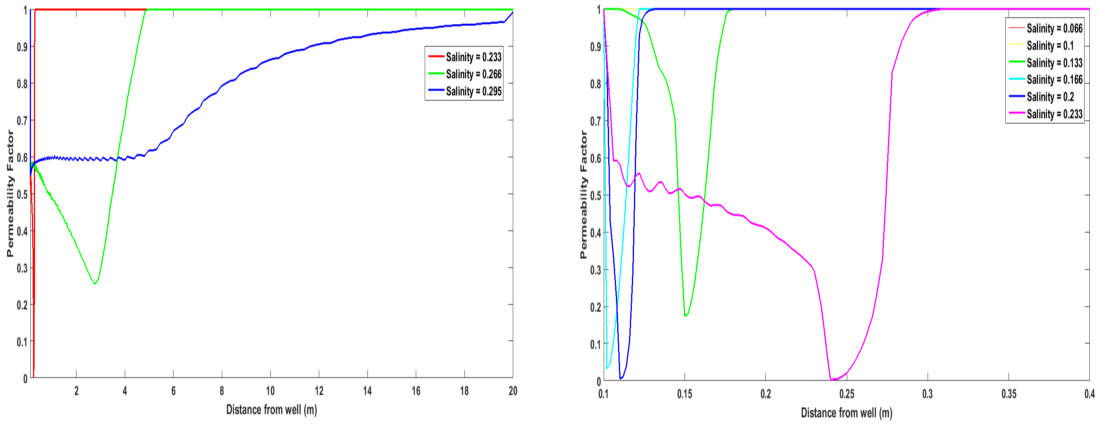

(a) Formation water salinity sensitivity - High salinity (Time = 3E07 s)

(b) Formation water salinity sensitivity - Low salinity (Time = 1E07 s)

Figure 4-14: Initial salinity sensitivity - K-Factor comparison (Solubility Limit = 0.295)

Fig. 4-14 depicts the sensitivity of the K-Factors to changes in salinity of the formation water. Fig. 4-14a depicts the sensitivity of the model towards high values of salinity and Fig. 4-14b towards low values of salinity. It can be observed that there is a certain trend in the sensitivity of the higher salinities, wherein salt precipitates with a comparatively slower rate and farther away from the wellbore, for a reservoir containing formation water of a higher salinity. However no such trend can be interpreted from Fig. 4-14b. A parameter study giving the dependence of liquid density, liquid viscosity and the rate of evaporation on the salinity is required to provide a concrete interpretation of the plots shown in Fig. 4-14. For the purposes of a sensitivity analysis, the expected behaviour of the model towards different salinities is detailed below.

As the salinity of formation water increases, the density and viscosity of formation water increases. An increase in the density and viscosity of the formation water results in a decrease in its mobility and thus a decrease in the rate of transport of the liquid. Furthermore, an increase in the salinity results in a decrease of the vapor pressure, as mentioned in equation 2-1. The impact of including vapor pressure lowering due to salinity is depicted in Fig. 4-15. It can be seen that vapor pressure lowering is of paramount importance in determining the location of salt precipitation. A decrease in the vapor pressure results in less amount of vapor being present in the gas and in turn leads to a lowered rate of drying.

It can thus be seen that an increase in salinity results in a decrease of both the drying and transport rates. The extent to which the rates of drying and transport are reduced depends on the dependence of the specific parameters mentioned above, on the salinity. An increase in salinity can thus convert the regime prevalent in the reservoir from a drying dominated regime to a transport dominated one and vice-versa.

Fig. 4-14a indicates that the reservoir is almost in a drying-transport balance at a salinity of 0.233. An increase in salinity results in a transition to a drying dominated regime, which

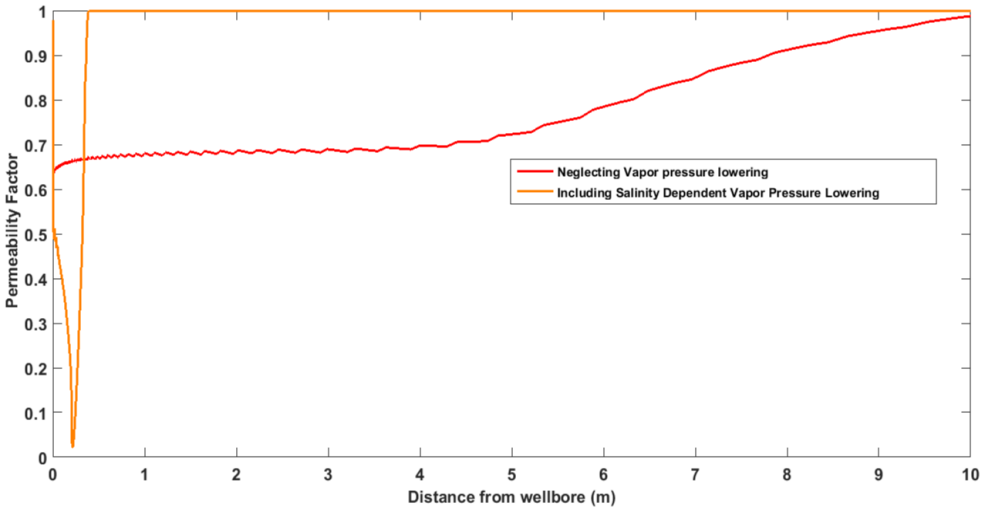

Figure 4-15: Impact of vapor pressure lowering on the salt precipitation profile

forces the salt precipitation profile to move away from the wellbore until it contributes to a pressure drop which can establish a drying transport balance.

Fig.4-14b is a bit more ambiguous to interpret, since there is no clear trend arising from an increase or decrease in salinities. However, by taking a closer look, it can be observed that all the salt precipitation is very close to the wellbore and the difference in location of the precipitation peaks are approximately 2.5 cm apart. It can thus be concluded that formation waters with lower salinities achieve the drying-transport balance very quickly and slight change in location of precipitation arises from the dependence of density, viscosity and vapor pressure on the salinity (see Equations 2-1, 3-12 and 3-13). The salinities of 0.066 and 0.1 are not observable in the figure, since formation waters with such levels of salinities need to undergo drying for an extended period to reach the solubility limit, before precipitation can ensue.

4-2-6 Sensitivity to the Bottom Hole Pressure

The bottom hole pressure is a variable which can be controlled on the surface. It is thus interesting to find out if producing at a particular bottom hole pressure can delay salt clogging in a well, through a sensitivity analysis.

Fig. 4-16 depicts the sensitivity of the model towards varying bottom hole pressures. It can be observed that near the wellbore, there is a clear trend, wherein the higher BHP's (or lower drawdowns) achieve the drying-transport balance earlier and results in a quicker clogging. Moving away from the wellbore, it can be observed that this trend starts to reverse for the higher drawdowns. The sensitivities shown in Fig. 4-16 is very similar to the one shown in Fig. 4-9 for sensitivity to reservoir pressure. The K-Factor trends are also very similar. The main difference arises from the fact that the simulations carried out in Fig. 4-9 clogs earlier when compared to the simulations carried out in Fig. 4-9, even when the drawdowns maintained are the same in both cases. Further analysis revealed that this difference was occurring due to the difference in gas expansion in the two cases.

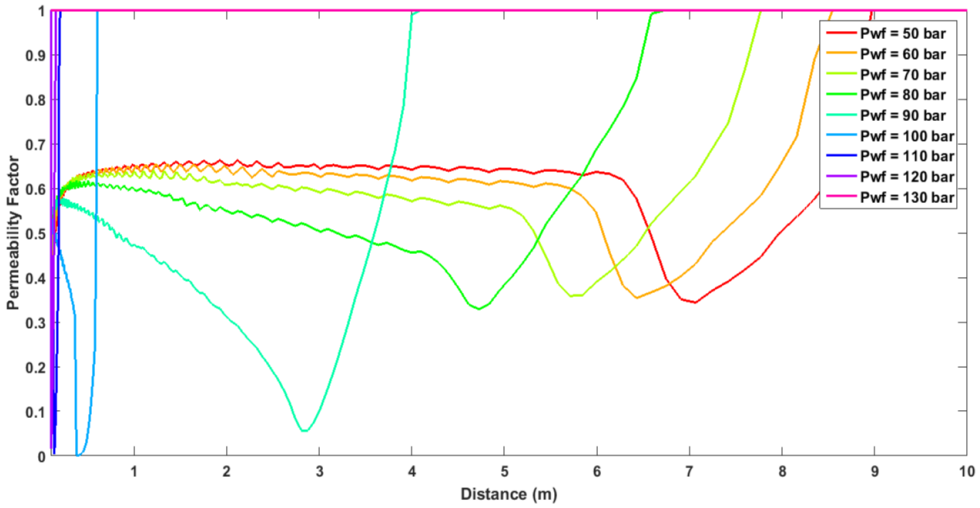

Figure 4-16: Bottom Hole Pressure sensitivity - Comparison of permeability factors (p_r = 140 bar) (Time = 3E07 s)

The amount of gas expansion occurring in a relatively high pressure reservoir (p_r = 170 bar), with a drawdown of 70 bar was found to be higher than the amount of gas expansion occurring in a moderately pressured reservoir (p_r = 120 bar), with a drawdown of 70 bar. A higher value of gas expansion results in a higher rate of drying and thus the drying transport balance will only be achieved later in time, thus prolonging clogging. This is the main difference that can be observed between the two aforementioned figures.

Another interesting feature which can be observed in Fig. 4-16 among others, is the presence of two precipitation peaks for the higher drawdowns. One peak close to the wellbore and another one away from the wellbore. The presence of these two peaks brings to light the question whether the downhole fresh water treatments currently being performed by the operators of these gas fields is dissolving both these salt precipitation peaks. It has been observed in the field that the frequency of water washing increases as the reservoir matures. The presence of this possibly unwashed precipitation peak can be one of the reasons for this increasing frequency of water washes required.

4-3 Effect of Capillary Film Flow

Capillary film flow has been neglected in the majority of the simulation carried out in this work, because it is unclear from literature how the capillary pressure and relative permeability curves have to be modelled in order to account for the effect of film flow. However, the literature in section 2-4 suggests that capillary film flow is a major transport mechanism in flow-through drying. Therefore the relative permeability curves were regularised below the apparent residual saturation (Fig. 3-2) according to the study conducted by Le and Mahadevan [2011], in order to perceive the impact of film flow on the salt precipitation profile.

Fig. 4-17 shows the impact of film flow on the salt precipitation profile. The line where the k_r is regularized, shows the impact of film flow. It can clearly be observed that including

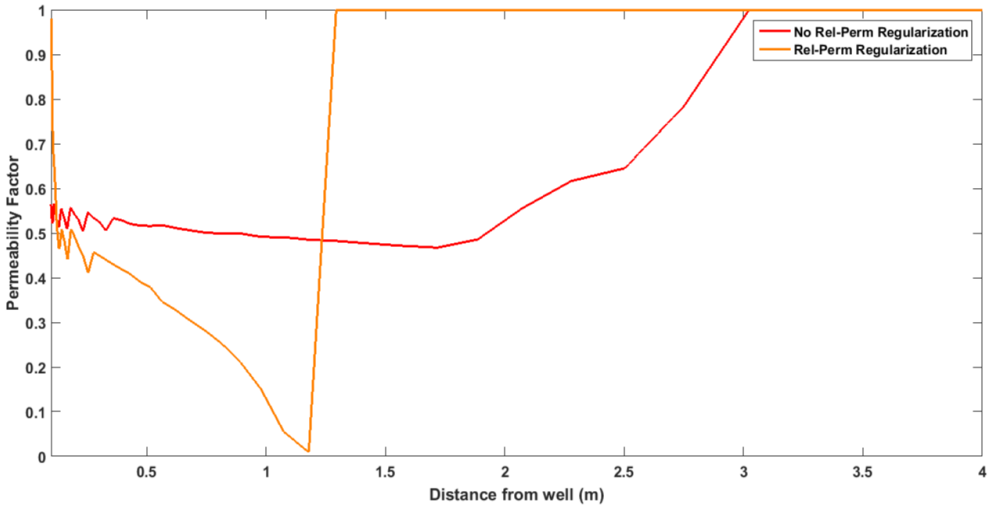

Figure 4-17: Impact of capillary film flow on the salt precipitation profile

film flow makes salt precipitation a nearer to wellbore phenomenon and also leads to quicker clogging.

The results and discussion for this phenomenon is similar to that explained in section 4-2-3. The presence of capillary film flow causes the drying-transport balance and thus salt clogging to happen earlier and closer to the wellbore. These results corroborate field observations, wherein salt clogging is mainly a near wellbore phenomenon. This suggests that a clear understanding of how capillary film flow can be modelled can help predict the salt precipitation location and timescales better.

4-4 Water Washing

Downhole fresh water treatments is currently the most common method used to dissolve precipitated salt and restore production from salted gas wells.

Dissolution of precipitated salt in DuMu^X is modelled as given in subsection 3-1-2. Water wash simulations carried out in DuMu^X suggests that the time required to restore the reservoir to its unaltered permeability state depends on three main parameters: The over pressure (p_w - p_r) maintained during the water wash, the radius of salt precipitation and the K-Factor reached during precipitation. The last two parameters are used to loosely describe the volume of precipitated salt.

A parameter study can be used to describe more accurately the dependency of time required for the water washing, on the aforementioned parameters.

Chapter 5

Optimization of the Production - Washing Cycle in Gas Wells with Salt Plugging

The main goal of almost all effort spent on modelling a petroleum reservoir is to devise an optimal strategy to develop, operate and manage the reservoir. Optimization of production operation can be instrumental in increasing recovery and reducing costs. This chapter gives an overview of the model developed to optimize the gas production from wells plagued with salt precipitation. Additionally, an optimization problem is formulated. The last section shows the scope for optimization of wells with salt precipitation and how a good reservoir management strategy can benefit the operators of these gas fields.

The salt precipitation model developed in DuMu^X (see chapter 3) is a steady-state near wellbore flow model (extending up to 20m away from wellbore) used to understand the physics underlying the salt precipitation phenomenon and its dependence on certain input parameters. It was observed during the study of this model that the salt precipitation and clogging process is very sensitive to certain parameters. This poses the question whether there is a possibility of managing certain parameters to mitigate the salt precipitation issue (In other words, does there exist an optimized reservoir management strategy which can maximize the productivity of gas reservoirs plagued by the salt precipitation issue?). In order to answer this question, a simplified full scale analytical reservoir model was developed in MATLAB, which draws upon the salt precipitation trends seen during numerical simulation in DuMu^X and represents it in the form of wellbore pressure drop due to skin. Furthermore, this analytical model describes a semi-steady state, single phase porous media flow of gas (CH4) under isothermal conditions.

5-1 Optimization Model

This simplified salt precipitation model considers a homogeneous reservoir with a declining reservoir pressure. The dependence of skin on the drawdown, wellbore pressure and time is

established though multiple DuMu^X simulations, by varying the bottom hole flowing pressures and drawdowns whilst keeping the rest of the parameters constant. Gas production is simulated for a fixed time period (T_{life}). As time progresses, the gas production declines and can drop below a critical gas production limit ($q_{g,crit}$), due to salt precipitation. This value of $q_{g,crit}$ is user defined. Additionally, a downhole fresh water treatment (water wash) is triggered whenever the gas production drops below the $q_{g,crit}$. It is assumed that this water wash dissolves all the salt precipitated and returns the reservoir to its unaltered permeability state. The duration of water washing is currently user defined and can be made dependent on the skin during further development of this model.

5-1-1 Mathematical model

The analytical model uses the p squared formulation to compute the gas flow rate at a given average reservoir pressure. The flow of control in the model is described below.

1. The total simulation time is discretized into 'n' equal time steps, since semi-steady state is being modelled.

2. The gas flow rate at the surface(q_g) is computed for every time step by using the formula:

$$q_g = \frac{\pi k_g h({p_{r,av}}^2 - {p_{wf}}^2)}{\mu_g B_g p_{r,av}(log\frac{r_e}{r_w} - \frac{3}{4} + S)}, \tag{5-1}$$

   where $p_{r,av}$ denotes the average reservoir pressure, B_g, the formation volume factor of gas, r_e and r_w, the external and wellbore radii respectively, S, the skin factor and k_g, the effective permeability of gas.

3. In the semi-steady state, the reservoir pressure declines with gas production. The new average reservoir pressure after production for a time step is given by:

$$p_{r,av_{i+1}} = p_{r,av_i} - \frac{B_g q_{g,sc} t}{c_g A h \phi}, \tag{5-2}$$

   where c_g denotes the gas compressibility, t, the time elapsed in one timestep and A stands for the cross sectional area of the reservoir.

4. The skin factor has been calculated according to the hawkin's formula as given below:

$$S = \left(\frac{K}{K_s} - 1\right) ln\frac{r_s}{r_w}, \tag{5-3}$$

   where K_s denotes the impaired permeability around the wellbore due to salt precipitation and r_s, the impaired permeability zone radius.

5. The variables K_s and r_s are unknown and are approximated from DuMu^X simulations. This approximation is carried out as follows:

   - Multiple DuMu^X simulation are run with a constant bottom hole pressure and varying reservoir pressures.
   - The previous step is repeated for varying bottom hole pressures

- For each simulation carried out, the lowest value of K-Factor($\frac{K_s}{K}$) is recorded for each timestep. The value of r_s corresponding to this lowest value of K-Factor is recorded for each time step as well
- From the data recorded in the previous step, plots of K_s v/s time and r_s v/s time can be generated (see Fig. 5-1).

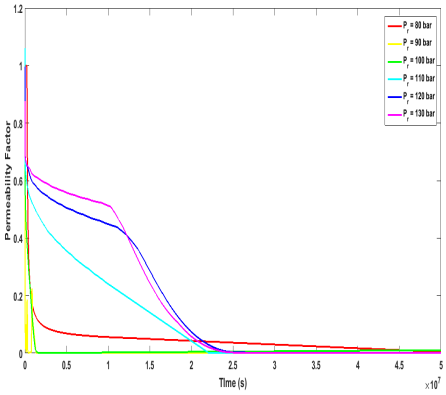

(a) Plot of K-Factor v/s time for a p_{wf} = 70 bar

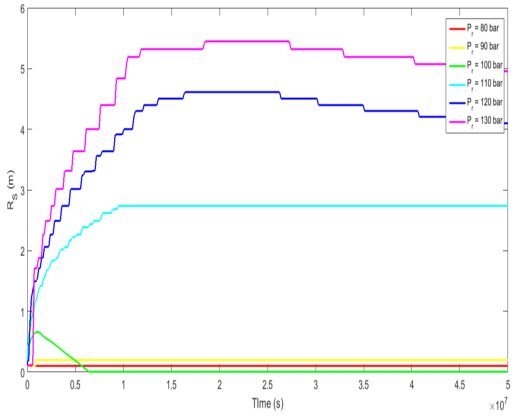

(b) Plot of r_s v/s time for a p_{wf} = 70 bar

Figure 5-1: Plot of K-Factor and r_s vs time

6. The skin factor is now formulated as a function of $p_{r,av}$, p_{wf} and time. The skin factor for a particular value of reservoir and bottom hole pressures for each timestep is found out through linear interpolation. The skin factor for the current timestep is used in equation 5-1, to compute the production decline due to salt precipitation.
7. When the value of gas production decreases below a pre-determined critical value ($q_{g,crit}$), a water wash is triggered.
8. The water wash is modelled in such a way that it is conducted for a fixed time period and the well is shut down for the duration of the wash. At the end of the wash, the skin factor is reset to zero and the reservoir is thus restored to its unaltered permeability state.
9. This washing production cycle continues for as long as the user desires or until the reservoir pressure declines to the point that it cannot produce above the critical gas production limit ($q_{g,crit}$).

5-1-2 Model Improvement

There are some developments which can be made to make this optimization model more accurate.

1. Flow rate calculations are currently not implemented in DuMu^X. Once these calculations are implemented, the flow rate measurements can be coupled to an analytical gas reservoir model to compute the change in skin factor with time more accurately.

2. It has been observed that the gas mobilities obtain higher values during the initial stages of salt precipitation. This is because a decreasing value of the liquid saturation results in a lower liquid relative permeability and consequently a higher value for the gas relative permeability. These trends are currently not implemented in the optimization model. Therefore, including the gas mobility trends can make the model more accurate.

3. The pseudo pressure formulation is a more accurate formulation to calculate the analytical gas flow rates. This formulation has been implemented in the optimization model, but has found to be computationally more time consuming than the p squared formulation shown in equation 5-1. A compromise has to be achieved between the computational cost and accuracy, for the optimization model.

5-2 Optimization Formulation

Optimization is concerned with the maximization or minimization of a function, subject to some control variables and constraints. The main elements in the formulation of the optimization of Net Present Value (NPV) of a single salt precipitating well as a mathematical problem are introduced here.

5-2-1 Objective function

As mentioned in 5-2, the objective of the optimization problem is to maximize the Net Present Value (NPV) of a single gas producing well. Furthermore, this production well is subject to intermittent shut downs and water injection in the form of water washes to dissolve precipitated salt. The general expression for the objective function is given below.

$$J(u) = \int_0^{T_{life}} \sum_{p=1}^{2} W_p(t) Q_p(t) dt, \tag{5-4}$$

where

- $[0, T_{life}]$ is the life cycle period
- Subscript p denotes the fluid phase (Gas or Water)
- $Q_p(t)$ is the surface volume rate of phase p at $t \in [0, T_{life}]$.
- $W_p(t)$ is a time dependent weight factor
- u is a vector of control variables

The expression for the weight factor is as follows:

$$W_p(t) = C_p \frac{1}{(1+r)^{(t)}}, \tag{5-5}$$

where

- C_p is the unit price ($\$/m^3$) of a fluid phase
- r is the annual discount rate

The unit prices (C_p) are positive for gas production and negative for water production and injection.

Equation 5-4 can be expanded to read:

$$J(u) = \int_0^{T_{life}} W_g(t)Q_g(t)dt + \int_0^{T_{life}} W_w(t)Q_w(t)dt, \tag{5-6}$$

where the subscripts w and g refer to the water and gas phase respectively.

5-2-2 Variables

The following key control variables are identified to be critical with respect to the production from a single well:

- The bottom hole pressure (p_{wf})
- The critical gas rate ($q_{g,crit}$)
- The life cycle of production (T_{life})

The control variable vector then becomes:

$$u = (p_{wf}, q_{g,crit}, T_{life}) \tag{5-7}$$

Bounds

Constraints have to be placed on the control variables, so that the optimization doesn't return a trivial or physically unrealistic solution.

The bottom hole pressure must be higher than the sum of the wellhead pressure and the pressure drop due to flow of gas up the wellbore. In the case of the salt precipitation model, the bottom hole pressure is additionally restricted to be below 100 bar. The critical gas rate must be higher than zero and lower than the initial gas production from a skin free reservoir. Furthermore the life cycle of the reservoir must be higher than zero and lesser than a user input value of T_{life}.

Therefore,

$$10 \leq p_{wf} \leq 100bar \tag{5-8}$$

$$0 \leq q_{g,crit} \leq Q_g(0) \tag{5-9}$$

$$0 \leq T_{life} \leq t_{end} \tag{5-10}$$

Changing bottom hole pressures

Furthermore, an additional optimization problem was formulated where the bottom hole pressures are varied every time step, to see if it gives a better optimized solution than setting just one value for the bottom hole pressure throughout the life of the reservoir. In this case, $p_{wf} = (p_{wf,1},\ p_{wf,2}, ., ., ...p_{wf,ntsteps})$, where $ntsteps$ denotes the number of timesteps.

A point of improvement of the optimization formulation would be to assign different bottom hole pressures after each washing cycle. This is more practical than assigning a different bottom hole pressure for each timestep. However there is a problem associated with this strategy. The number of bottom hole pressures as control variables would depend on the number of washing cycles performed. Now, since the number of washing cycles is in itself a variable, this strategy would result in a variable number of control variables, which cannot be handled straightforwardly by optimizers, as they expect a fixed number of variables.

In the case of changing bottom hole pressures with each time step, the control variable vector then becomes:

$$u = (p_{wf,1},\ p_{wf,2}, ., ., ...p_{wf,ntsteps}, q_{g,crit}, T_{life}) \tag{5-11}$$

5-3 Scope for Optimization

A number of simulations were run on the analytical optimization model detailed in section 5-1, in order to assess if this model is suitable for optimization purposes and to see if the simulations relate to field observations. The input parameters are shown in appendix A-2 and are not changed in any of the following simulations, unless specified otherwise. The results are shown below.

5-3-1 Frequency of Washing

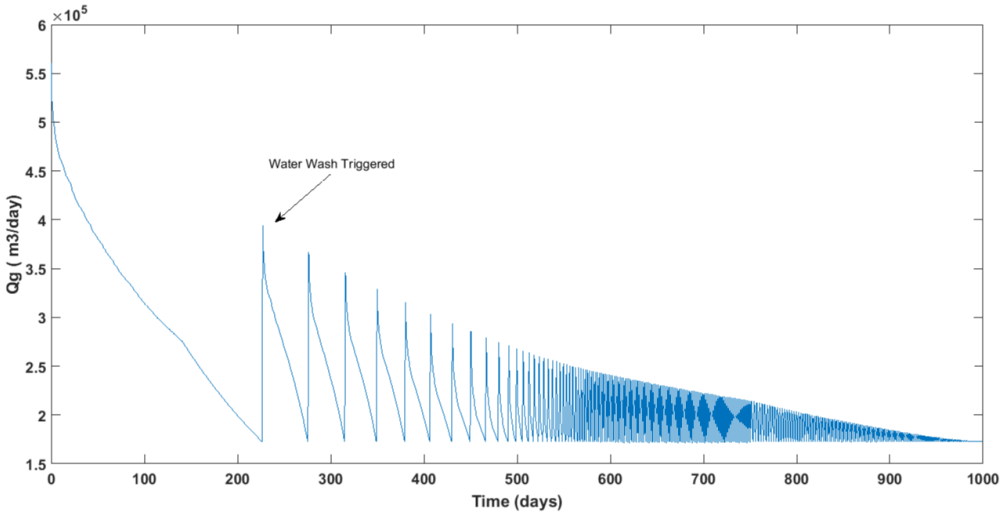

Figure 5-2: Plot depicting increase in the frequency of water washes with time

Fig. 5-2 shows a situation where the reservoir was produced initially with a drawdown of 50 bar. The reservoir depletes over the course of 1000 days. An increase in the frequency of water washes required to produce the reservoir can be observed and can be corroborated by field observations reported by the operators of gas fields.

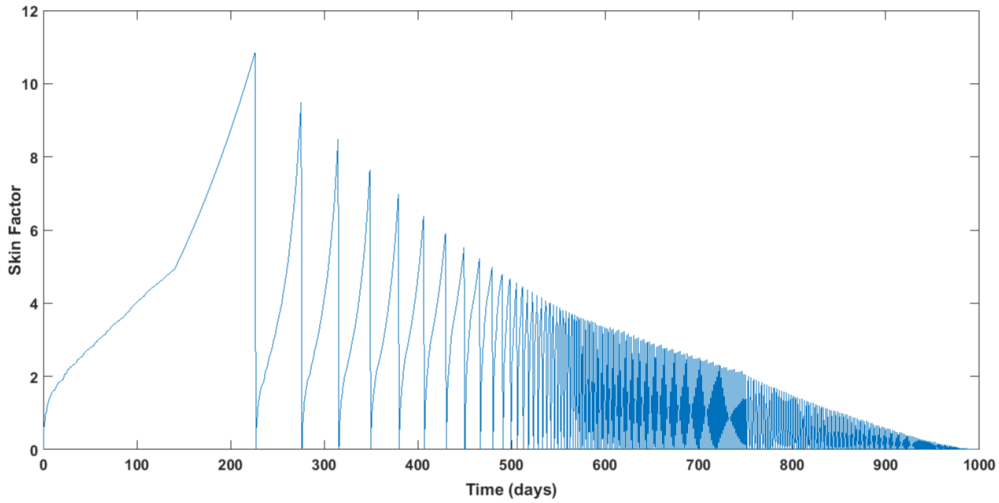

Figure 5-3: Development of skin over 1000 days

Fig. 5-3 shows the development of skin over the course of time. It can be observed that as the reservoir pressure declines, the skin develops faster.

5-3-2 Optimization opportunity

p_{wf} as a control variable

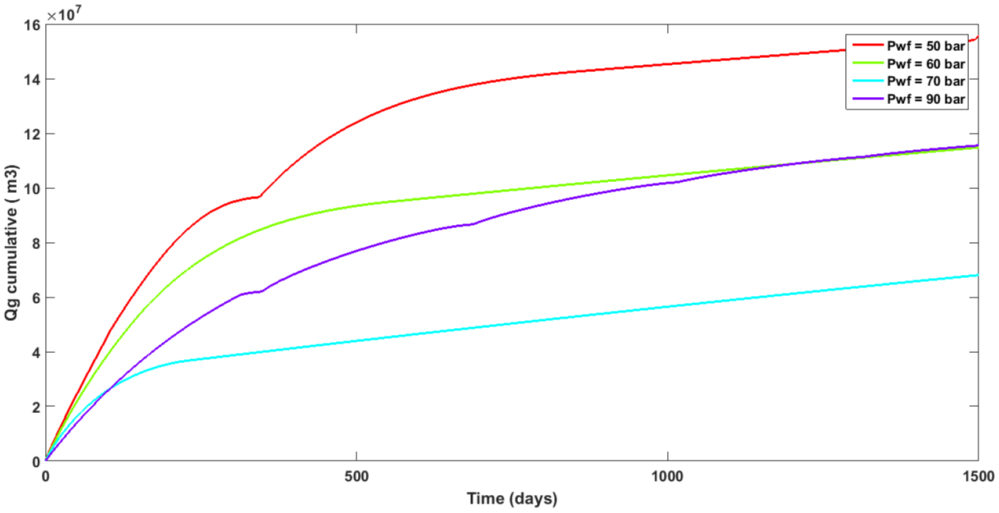

Figure 5-4: Base Case Simulation : Comparison of cumulative gas production for four different FBHP's

A comparison of cumulative gas production for four different FBHP's can be seen in Fig. 5-4. The reservoir pressure is 110 bar. The value for $q_{g,crit}$ has been taken to be 0.2 m^3/s in this simulation.

We can observe that the lowest drawdown case ($p_{wf} = 90$bar) attains a higher cumulative gas production in the model compared to FBHP's (Flowing Bottom Hole Pressure's) of 70 and 60 bar, which is interesting from an optimization point of view and suggests that producing at the highest drawdown need not be the best strategy.

$q_{g,crit}$ as a control variable

It is interesting to see if the decision regarding the value of $q_{g,crit}$ can make significant changes in the cumulative gas produced.

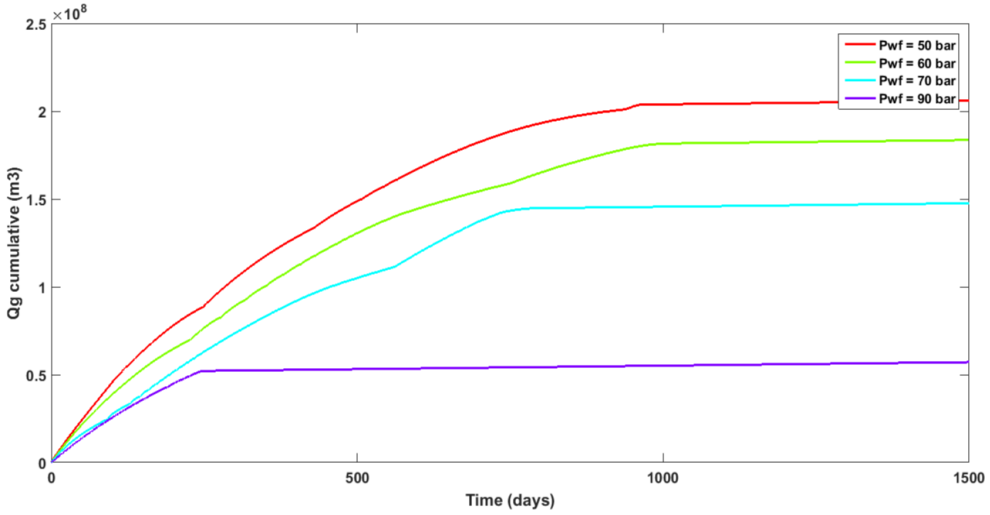

Figure 5-5: Cumulative gas production for a $q_{g,crit}$ of 2 m^3/s

The figures 5-4 and 5-5 depict simulations in which $q_{g,crit}$ has been increased from 0.2 m^3/s to 2 m^3/s respectively. It can be observed that certain $q_{g,crit}$ values give a higher value of gas production, for certain initial FBHP values. In this case, the $q_{g,crit}$ value of 2 m^3/s gives a higher overall value for the cumulative gas produced. This shows that $q_{g,crit}$ can be considered as an control variable.

In Fig. 5-5 it can be observed that the cumulative gas production for the inital FBHP of 90 bar flat lines after a short duration. This is because the reservoir pressure has declined to such an extent that it can't produce at a rate higher than the $q_{g,crit}$.

Life Cycle Optimization

Fig. 5-6 depicts a situation where the reservoir has been produced for a life time of 10000 days. It can be observed that the highest initial FBHP case gives the highest cumulative gas produced over the life time of the reservoir. These trends are contrary to the trends observed in Fig. 5-4 and shows that the T_{life} is a crucial parameter for deciding the gas production strategy.

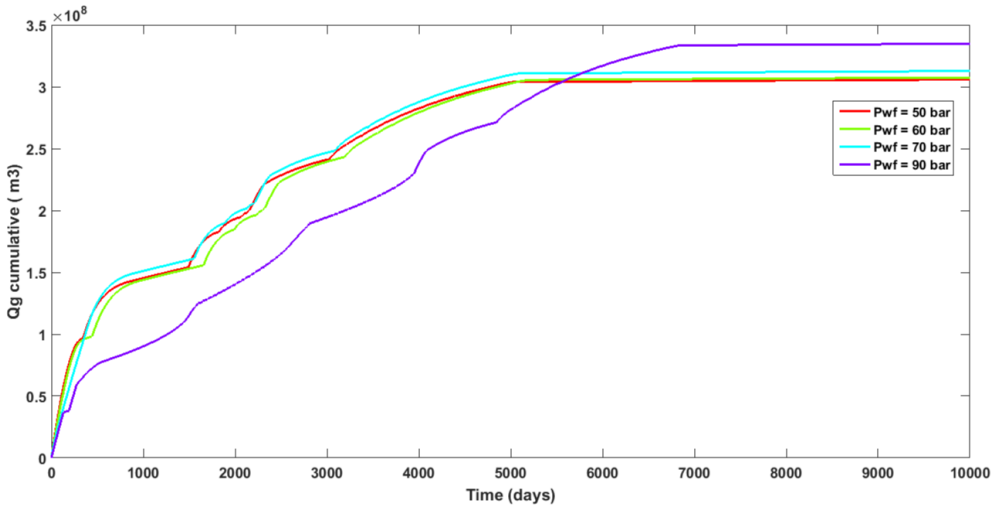

Figure 5-6: Cumulative gas production comparison for a reservoir life of 10000 days

Furthermore, since the frequency of washing increases with time, it will not be profitable to continue producing gas after a period of time. Thus it makes sense to introduce T_{life} as a control variable.

Changing p_{wf} for each time step

Setting the value of the FBHP to an optimized value for each timestep will give the best optimization strategy for salt precipitating wells. In order to show that changing the FBHP for each timestep can indeed improve the cumulative gas produced, a simplified example is shown in Fig. 5-7, wherein the FBHP is reduced in accordance with the decline in reservoir pressure, so as to maintain a constant drawdown in the reservoir. Please note the lower bound for the FBHP is set at 50 bar.

On comparing Fig. 5-4 and Fig. 5-7, it can be observed that for the case of initial FBHP = 70 bar, changing the value of FBHP at each timestep results in a significantly higher value of cumulative gas produced. This gives an indication that setting the FBHP to an optimized value for each timestep will theoretically give the most optimized value for the cumulative gas produced. A more practical approach would be to set a different value for the FBHP after each washing cycle.

Influence of Water Wash Duration on Q_g

The amount of time required for a single water wash to return the reservoir to its unaltered permeability state has been take to be a constant in all the simulations carried out here.

In essence, the washing duration is a variable and depends on the amount of salt that has been precipitated during the gas production cycle. Development of a more detailed washing model, wherein the washing duration is dependent on the skin factor, can result in the washing duration being a control variable.

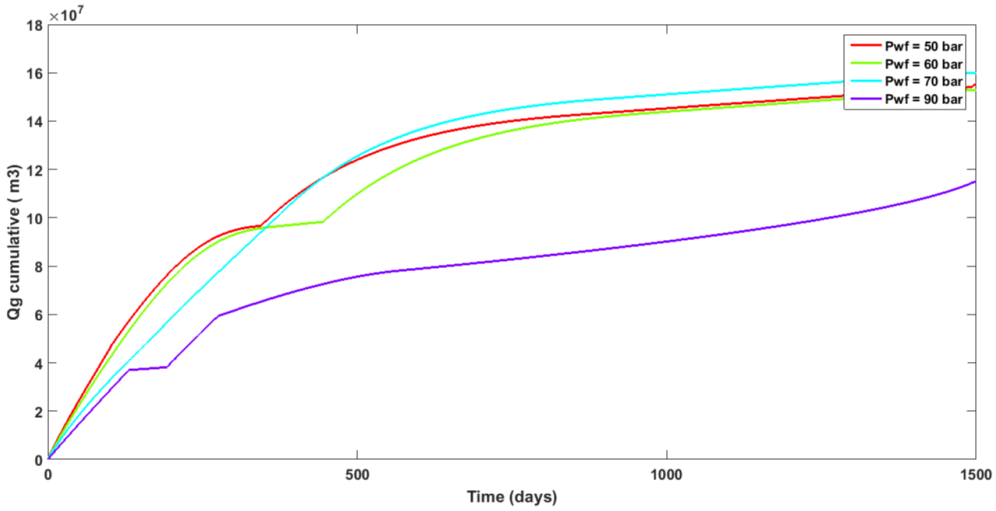

Figure 5-7: Base case simulation with drawdown maintenance - Cumulative gas production comparison

Chapter 6

Conclusions

In this work, the mechanisms underlying near wellbore salt precipitation in gas reservoirs have been investigated to get a better understanding of this phenomenon.

This has been carried out by conducting sensitivity analyses to measure the dependence of salt precipitation on certain critical parameters. Based on these results, a drying-transport balance hypothesis was developed, which can explain the variation in the salt precipitation trends both in time and in space. Furthermore, the possibility of having an optimized reservoir management strategy, which can better the cash flow from wells having salt deposition, was investigated. Based on these results, a simplified analytical model was developed to show the scope for optimization. Furthermore, an optimization problem was formulated to maximize the Net Present Value (NPV) of wells undergoing cyclic production and water washing.

The location of salt precipitation in a reservoir has been found to be heavily dependent on a number of parameters. These parameters include those contributing to both evaporative drying and liquid transport. Even though the salt precipitation model is very sensitive to many parameters, complete clogging of the pore throats with salt was only found to be possible when the reservoir achieves a drying-transport balance. Furthermore, presence of capillary wicking was found to highly influence the location of salt precipitation.

The sensitivity of the model to changing reservoir and bottom hole pressures revealed that producing at the highest drawdown may not be the best strategy, since higher drawdowns were found to clog earlier in time, under certain conditions.

The bottom hole pressure, the critical gas rate and the life cycle of the reservoir were identified as control variables for optimizing the NPV of cyclic production and injection process in a well with salt clogging.

6-1 Recommendations

- A better understanding of the behaviour of the capillary pressure curve below the apparent residual saturation is required for a more precise prediction of the location of salt precipitation.

- The salt precipitation model introduced in this thesis should be expanded to include other dissolved salts apart from NaCl.
- The inclusion of gravity in the salt precipitation model will give an idea about the location of salt precipitation along the height of the reservoir.
- It would be interesting to see if a relationship between the input parameters and the salt precipitation location and timescale can be derived based on a parameter study.
- For the purpose of optimization, a better alternative to the Hawkins skin model would be to use flow rates from DuMu^X as an input to a two phase analytical formulation, in order to calculate the skin development with time.
- The possibility of formation of water blocks during the flow back of injected water should be investigated.

Appendix A

Appendix

A-1 Spatial Discretization in DuMu^x

In the salt precipitation model, the spatial discretization of the domain is carried out by DuMu^X, using the BOX method. "The BOX method unites the advantages of the finite-volume(FV) and the finite-element(FE) methods" Leh [2014]. A short introduction to the Box method, as given in Leh [2014], is described below.

The model domain G is initially discretized with a FE mesh, having nodes i and corresponding elements E_k. A secondary FV mesh is then constructed by joining the midpoints with the barycenters of the elements surrounding node i, thereby creating a box B_i around the node i (see Fig. A-1a). The box B_i is divided into subcontrolvolumes (scv's), by the FE mesh. (see Fig. A-1b). Fig. A-1c, represents the finite element E_k and the scv's b_i^k inside E_k. It can be seen that the scv's inside E_k belong to four different boxes B_i. The other parameters shown in Fig. A-1c, and necessary for the discretization are the faces of the subcontrolvolumes (scvf's) e_{ij}^k between the scv's b_i^k. $|e_{ij}^k|$ is the length of the scvf, x_{ij}^k are integration points on e_{ij}^k and n_{ij}^k is the outer normal vector.

The advantage of using the box method is that it combines the mass conservation aspect of the FV method with the possibility of using unstructured grids, since the FE method is also used. The idea is to apply the FV method to each FV box B_i and to get the fluxes across the interfaces e_{ij}^k, at the integration points x_{ij}^k from the FE approach. This results in the following expression at each scvf:

$$f(\tilde{u}(x_{ij}^k)) \cdot \mathbf{n}_{ij}^k \; |e_{ij}^k| \qquad \text{with} \qquad \tilde{u}(x_{ij}^k) = \sum_i N_i(x_{ij}^k \cdot \hat{u}_i). \tag{A-1}$$

The Reynolds transport theorem gives the general balance equation:

$$f(u) = \int_G \frac{\partial u}{\partial t} \; dG \; + \; \int_G \nabla \cdot [\mathbf{v}u + \mathbf{w}(u)] \; dG - \int_G q \; dG = 0 \tag{A-2}$$

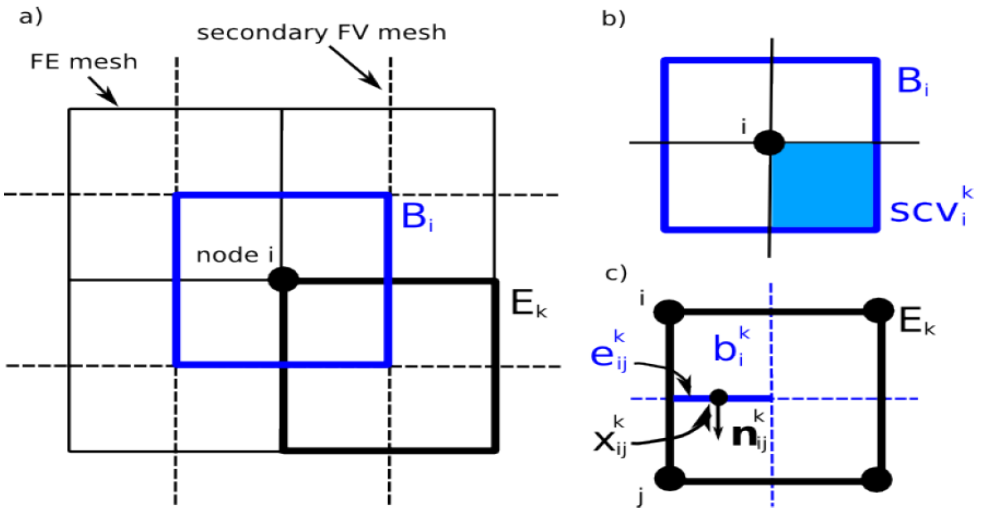

Figure A-1: The BOX discretization scheme(from Leh [2014]

The box method follows the principle of weighted residuals. The unknown u in the function $f(u)$ is approximated by a FE approximation, given by:

$$\tilde{u} = \sum_i N_i \hat{u}_i, \tag{A-3}$$

where $u \in \{\mathbf{v}, p, x^k\}$, $\hat{u}_i$ are discrete values at the nodes of the FE mesh and N_i is a linear basis function. Due to this approximation with node values and basis functions, a residual ε is produced.

$$f(u) = 0 \qquad \Longrightarrow \qquad f(\tilde{u}) = \varepsilon \tag{A-4}$$

The principle of weighted residuals, implies that the multiplication of the residual ε with a weighting function W_j should lead to value of zero over the whole domain.

$$\int_G W_j \cdot \varepsilon \stackrel{!}{=} 0 \quad \text{with} \quad \sum_j W_j = 1 \tag{A-5}$$

A mas lumping technique is then applied, which assumes that the storage capacity is reduced to the nodes. This is carried out by the introduction of a mass lumping term $M_{i,j}^{lump}$ which is defined as:

$$M_{i,j}^{lump} = \begin{cases} \int_G W_j \; dG = \int_G N_i \; dG = V_i & i = j \\ 0 & i \neq j \end{cases} \tag{A-6}$$

Furthermore, the weighting function W_j is assumed to be piecewisely constant over control volume box B_i

$$W_j(x) = \begin{cases} 1 & x \in B_i \\ \\ 0 & x \in B_i \end{cases} \tag{A-7}$$

causes ∇W_j to be zero. Finally, the consideration of time discretization and inserting the value of W_j as 1, leads to the discretized form (Equation A-8), which will be applied to the mathematical flow and transport equations.

$$V_i \frac{\hat{u}_i^{n+1} - \hat{u}_i^n}{\Delta t} + \int_{\partial B_i} F(\tilde{u}^{n+1}) \cdot \mathbf{n} \, d\Gamma_{B_i} - V_i q^{n+1} = 0 \tag{A-8}$$

A-2 Base case input parameters for the analytical optimization model (MATLAB)

```
ht = 20;              % Reservoir Thickness (m)
k_g = 22.3E-15;       % Effective gas permeability (m2)
p_R = 110E5;          % Average Reservoir Pressure (Pa)
p_wf = 60E5;          % Bottom Hole Flowing Pressure (Pa)
r_e = 1000;           % Drainage Radius (m)
r_w = 0.1;            % Wellbore Radius (m)
T_R = 418.15;         % Reservoir Temperature (K)
phi = 0.11;           % Porosity
T_life = 1500;        % End Time for simulation (days)
q_g_crit = 0.2;       % Critical gas rate to trigger well shut down
(m3/s)
```

A-3 Base case input parameters for sensitivity analysis (DuMu^X)

```
#####################################################################
# Mandatory arguments
#####################################################################
[TimeManager]
TEnd                = 30000000      # [s] duration of the simulation
DtInitial           = 10            # [s] initial time step size
MaxTimeStepSize     = 50000         # [s] maximum timestep #604800

#####################################################################
[Grid]
File                =   grid/pieceofcake20x20x1_10_nZrefined4.dgf
InnerRadius         = 0.1   # [m]
#OuterRadius        = 20.0  # [m]

#####################################################################
[FluidSystem]
NTemperature        = 3       # [-]  number of tabularization entries
NPressure           = 10000 # [-]  number of tabularization entries
PressureLow         = 1.0E4  # [Pa] low end for tabularization of fluid properties
PressureHigh        = 22.0E6 # [Pa] high end for tabularization of fluid properties
TemperatureLow      = 417.0  # [Pa] low end for tabularization of fluid properties
TemperatureHigh     = 420.0  # [Pa] high end for tabularization of fluid properties
VaporPressureMethod = 2       # [0] No vapor Pressure [1] No vapor pressure reduction [2] Vapor
pressure reduction according to Haas

#####################################################################
[Problem]
OutputFolder        = .//SalSensitivity//sals0.26//   # [-] ABSOLUTE PATH
OutputName          = sals0.26                        # [-]  name for output files

ReservoirPressure   = 11.0E6#10.0E6                   # [Pa] initial reservoir pressure
InnerNeumann        = 0                               # [-] 0: Dirichlet; 1: Neumann   2:Outflow
boundary, with gas phase pressure set according to dirichlet
InnerWatInjRate     = 0                               # [kg/m2/s] Negative value is flux into reservoir.
InnerGasInjRate     = 0                               # [kg/m2/s] Negative value is flux into reservoir.
InnerPressure       = 8.0E6                           # [Pa] well bhp
InnerLiqSaturation  = 0.0                             # [-] liquid saturation at inner boundary.
InnerSalinity       = 0.0                             # [-] salinity of injected liquid
OuterPressure       = 11.0E6                          # [Pa] reservoir boundary pressure
OuterLiqSaturation  = 0.35                            # [-]  liquid saturation at outer boundary
Temperature         = 418.15                          # [K]  reservoir temperature
Salinity            = 0.26                            # [-]  initial salinity
SaltPorosity        = 0                               # [-]  porosity precipitated salt
PermPorModel        = 3                               # [-]  (0) OFF [default] - (1) Kozeny-Carman - (2)
Verma-Pruess - (3) PowerLaw
PowerLaw_exponent   = 15                              # [-]  exponent of power law
VermaPruess_param   = 0.9                             # [-]  param for Verma-Pruess
```

```
LiquidSaturation        = 0.35              # [-]  initial liquid saturation
InitPrecipitatedSalt    = 1E-5              #[kg/m3]  initial precipitated salt

#####################################################################
[SpatialParams]
SolubilityLimit         =  0.295        # [-]  solubility limit of salt in brine
Porosity                =  0.11         # [-]  initial porosity
Permeability_1          =  2.23E-14     # [m2] initial permeability region1
Permeability_2          =  2.23E-14     # [m2] initial permeability region2
IrreducibleLiqSat       =  0.2          # [-]  irreducible liquid saturation
IrreducibleGasSat       =  0.001        # [-]  irreducible gas saturation
MaterialLaw             =  0            # [-]   [0] RegularizedBrookscorey  [1] TabularData  (Monotone
Spline)
##### Brooks and Corey parameters
BrooksCorey_Pe          =  3.85E4       # [Pa] entry pressure of BC law
BrooksCorey_Lambda      =  2            # [-]  lambda parameter of BC law
MinimalSaturationThreshold  = 0.01      # Below which the capillary pressure is regularized
CapillaryCorrection             = 1     # Dynamic Capillary pressure correction

#####################################################################
 [TimeManager]
#Restart                        = 864000
WriteRestartFile                = 0     # Boolean. Should restart files be written? (1) Yes (0) No

#####################################################################
[ Vtk ]
AddVelocity             = 1     # Add extra information
VtuWritingFreq          = 1     # 1: write a vtu file at every timestep, 2: write a vtu file every second
timestep ...

#####################################################################
[LinearSolver]
ResidualReduction = 1e-12

#####################################################################
[Newton]
RelTolerance = 1e-12

#####################################################################
[Implicit]
#EnableHints                            = "0"   #default: 0
#EnableJacobianRecycling                = "1"   #default: 1
#EnablePartialReassemble                = "1"   #default: 1
#MassUpwindWeight                       = "1"   #default: 1
#MaxTimeStepDivisions                   = "10"  #default: 10
#MobilityUpwindWeight                   = "1"   #default: 1
#UseTwoPointFlux                        = "0"    #default: 0
```

Bibliography

Exxon Mobil. Applications against nacl - scale at empg. November 2011.

V.A. Jambhekar, R. Helmig, N. Schröder, and N. Shokri. Free-flow-porous-media coupling for evaporation-driven transport and precipitation of salt. January 2015.

A.G. Yiotis, A.G. Boudouvis, A.K. Stubos, I.N. Tsimpanogiannis, and Y.C. Yortsos. The effect of liquid films on the drying of porous media. *AIChE Journal*, 50:2721–2737, 2004.

J.S. Ward and N.R. Morrow. Capillary pressure and gas relative permeability of low-permeability sandstone. *SPE Form Eval*, 2:345–356, 1987.

D. Le and J. Mahadevan. Productivity loss in gas wells caused by salt deposition. *SPE Journal*, pages 908–920, 2011.

P. Egberts. Comparison tough2/ewasg and dumu^x. October 2014.

DuMu^X Handbook. Lehrstuhl fur Hydromechanik und Hydrosystemmodellierung, Universitat Stuttgart, Paenwaldring 61, D-70569 Stuttgart, Germany, 2.6 edition, October 2014.

M.C. Place and J.T. Smith. An unusual case of salt plugging in a high-pressure sour gas well. In *SPE 59th Annual Technical Conference and Exhibition*. SPE, September 1984.

F.A.L. Dullien, C. Zarcone, I.F. MacDonald, A . Collins, and D.E. Bochard. The effects of surface roughness on the capillary pressure curves and the heights of capillary rise in glass bead packs. *Journal of Colloid and Interface Science*, 127:362–372, 1989.

S.A. Holditch. Factors affecting water blocking and gas flow from hydraulically fractured gas wells. *Journal of Petroleum Technology*, 31:1515–1524, 1979.

J. Kamath and C. Laroche. Laboratory-based evaluation of gas well deliverability loss caused by water blocking. *SPE Journal*, 8:71–80, 2003.

H.J. Dietzel, W. Kleinitz, and W. Littmann. Wiederherstellung der zuflussbedingungen nach aufwältigungs- und komplettierungsarbeiten in gasbohrungen. *Erdl Erdgas Kohle*, 11, 1993.

W. Kleinitz, M. Koehler, and G. Dietzsch. The precipitation of salt in gas producing wells. In *SPE European Formation Damage Conference, Hague, The Netherlands*. SPE, May 2001.

Q.T. van Dorp, M. Slijkhuis, and P.L.J. Zitha. Salt precipitation in gas reservoirs. In *SPE European Formation Damage Conference, Scheveningen, The Netherlands*. SPE, May 2009.

J. Mahadevan, M.M. Sharma, and Y.C. Yortsos. Capillary wicking in gas wells. *SPE Journal*, pages 429–437, 2007.

K.E. Newsham and J.A. Rushing. Laboratory and field observations of an apparent sub-capillary-equilibrium water saturation distribution in a tight gas sand reservoir. *SPE Gas Technology Symposium*, May 2009.

R. Tang and Y. Etzion. Comparative studies on the water evaporation rate from a wetted surface and that from a free water surface. *Building and Environment*, 39:77–86, 2004.

E. Zuluaga and J.C. Monslave. Water vaporization in gas reservoirs. *Paper SPE 84829 presented at the SPE Eastern Regional Meeting*, September 2003.

M Greensmith. *Practical Dehydration*. Woodhead Publishing Limited, 1998.

J. Mahadevan, M.M. Sharma, and Y.C. Yortsos. Flow-through drying of porous media. *AIChE Journal*, 52:2367–2380, 2006.

J. Allerton, L.E. Brownell, and D.L. Katz. Through-drying of porous media. *Chemical Engineering Progress*, 45:619–635, 1949.

J. Mahadevan and M.M. Sharma. Factors affecting cleanup of water blocks: A laboratory investigation. *SPE Journal*, 10:238–246, 2005.

A.V Luikov. *Heat and Mass Transfer in Capillary Porous Media*. Pergamon Press, 1966.

S. Whitaker and W.T.H. Chou. Drying of granular porous media - theory and experiment. *Drying Technology*, 1:3–33, 1983.

P. Coussot. Scaling approach of the convective drying of a porous medium. *The European physical journal B-condensed matter and complex systems*, 15:557–566, 2000.

E. Fisher. Some factors affecting the evaporation of water from soil. *The Journal of Agricultural Science*, 13:121–143, 1923.

U.. Nachshon, E.. Shahraeeni, D.. Or, M. Dragila, and N. Weisbrod. Infrared thermography of evaporative fluxes and dynamics of salt deposition on heterogenous porous surfaces. *Water Resources Research*, 47, 2011.

P. Lehmann, S. Assouline, and D. Or. Characteristic lengths affecting evaporative drying of porous media. *Physical Review E*, 77, 2008.

E.. Shimojimaa, R.. Yoshioka, and I.. Tamagawa. Salinization owing to evaporation from bare-soil surfaces and its influences on the evaporation. *Journal of Hydrology*, 178:109–136, 1996.

I. Nassar and R. Horton. Salinity and compaction effects on soil water evaporation and water and solute distributions. *Soil Science Society of America Journal*, 63:752–758, 1999.

H. Fujimaki, T. Shimano, M. Inoue, and K. Nakane. Effect of a salt crust on evaporation from a bare saline soil. *Vadose Zone Journal*, 5:1246–1256, 2006.

A. Battistelli, C. Calore, and K. Pruess. Vapor pressure lowering effects due to salinity and suction pressure in the depletion of vapor-dominated geothermal reservoirs.

K. Pruess and M.O. Sullivan. Effect of capillarity and vapor adsorption in the depletion of vapor-dominated geothermal reservoirs.

M. Goyeneche, D. Lasseux, and D. Bruneau. A film flow model to describe free water transport during drying of a hygroscopic capillary porous medium. *Transport in Porous Media*, 48: 125–158, 2002.

G.A. Spolek and O.A. Plumb. Capillary pressure in softwoods. *Wood Science and Technology*, 15:189–199, 1981.

M. Kaviany and M. Mittal. Funicular state in drying of a porous slab. *Int. J. Heat and Mas Transfer*, 30:1407–1418, 1987.

P. Perre and C. Moyne. Processes related to drying: part 2, use of the same model to solve transfers both in saturated and unsaturated porous media. *Drying Technology*, 9:1153–1179, 1991.

J.R. Puiggali and M. Quintard. Properties and simplifying assumptions for classical drying models. *Advances in Drying*, 5:131–147, 1992.

G.L. Comstock. Directional permeability of softwoods. *Wood Fiber*, 1:283–289, 1970.

C. Moyne. *Transferts coupls chaleur-masse lors du schage: prise en compte du mouvement de la phase gazeuse*. PhD thesis, University of Nancy, France, 1987.

C. Laroche, M. Chen, Y.C Yortos, and J. Kamath. Time scaling of rates of produced fluids in laboratory displacement. *SPE Journal*, 9:34–46, 2004.

P. Bastian, M. Blatt, A. Dedner, C Engwer, R. Klofkorn, R. Kornhuber, M. Ohlberger, and O. Sander. On the generic parallelisation of iterative solvers for the finite element method. *Computing*, 4:121–138, 2008.

B. Flemisch, M. Darcis, K. Erbertseder, B. Faigle, A. Lauser, K. Mosthaf, S. Muthing, P. Nuske, A. Tatomir, and M. and Wolff. Dumu^x: Dune for multi-phase, component, scale, physics, flow and transport in porous media. *Advances in Water Resources*, 34: 1102–1112, 2011.

M. Batzle and Z. Wang. Seismic properties of pore fluids. *Geophysics*, 57:1396–1408, 1992.

H. Class, R. Helmig, and P. Bastian. Numerical simulation of non-isothermal multiphase multicomponent processes in porous media: 1. an efficient solution technique. *Advances in Water Resources*, 25:533–550, 2002.

A. Lauser, C. Hager, R. Helmig, and B. Wohlmuth. A new approach for phase transitions in miscible multi-phase flow in porous media. *Advances in Water Resources*, 34:957–966, 2011.

R.H. Brooks and A.T. Corey. Hydraulic properties of porous media. *Hydrology Papers, Colorado State University*, March 1964.

S. Pavuluri. Kinetic approach for modelling salt precipitation in porous-media. Master's thesis, Stuttgart University, 2014.